

Robust Image Protection Countering Cropping Manipulation

Qichao Ying, *Student Member, IEEE*, Hang Zhou, Zhenxing Qian, *Member, IEEE*, Sheng Li, *Member, IEEE* and Xinpeng Zhang, *Member, IEEE*

Abstract—Image cropping is a cheap yet effective operation of maliciously altering image contents. Existing cropping detection mechanisms analyze the fundamental traces of image cropping, for example, chromatic aberration and vignetting to uncover cropping attack. However, they are fragile to common post-processing attacks which deceive forensics by removing such cues. Besides, they ignore the fact that recovering the cropped-out contents can unveil the purpose of the behaved cropping attack. This paper presents a novel robust watermarking scheme for image Cropping Localization and Recovery (CLR-Net). We first protect the original image by introducing imperceptible perturbations. Then, typical image post-processing attacks are simulated to erode the protected image. On the recipient's side, we predict the cropping mask and recover the original image. We propose two plug-and-play networks to improve the real-world robustness of CLR-Net, namely, the Fine-Grained generative JPEG simulator (FG-JPEG) and the Siamese image pre-processing network. To the best of our knowledge, we are the first to address the combined challenge of image cropping localization and entire image recovery from a fragment. Experiments demonstrate that CLR-Net can accurately localize the cropping as well as recover the details of the cropped-out regions with both high quality and fidelity, despite the presence of image processing attacks of varied types.

Index Terms—robust watermarking, image forensics, data hiding, crop localization, image recovery.

I. INTRODUCTION

WITH the exploding amount of images transmitted through the Internet, anyone can take a picture anywhere anytime. Digital images have largely replaced conventional photographs from all walks of life. The rapid advancements in digital image processing has made it extremely easy with the presence of user-friendly image editing software, and the edited images can be shared with others in seconds with social networking services. Although these advances have benefited people's lives, digital images can hardly enjoy the credibility of their conventional counterparts. Image forgery is the behaviors that deliberately alter the interpretation of the original image by modifying parts of its contents.

Manuscript received Jun 2, 2022; revised Sep 7, 2022; accepted XX, 2022. Date of publication XX, 2022; date of current version XX, 2022. Corresponding author: Zhenxing Qian.

Q. Ying, Z. Qian, S. Li and X. Zhang are with the School of Computer Science, Fudan University, Shanghai, China. Email: {qying20, zxqian, lisheng, zhangxinpeng}@fudan.edu.cn. H. Zhou is with the School of Computer Science, Simon Fraser University, British Columbia, Canada. Email: zhouhang2991@gmail.com.

This work is supported by National Natural Science Foundation of China under Grant U20B2051, U1936214. We are grateful to the reviewers for their constructive suggestions in improving this paper.

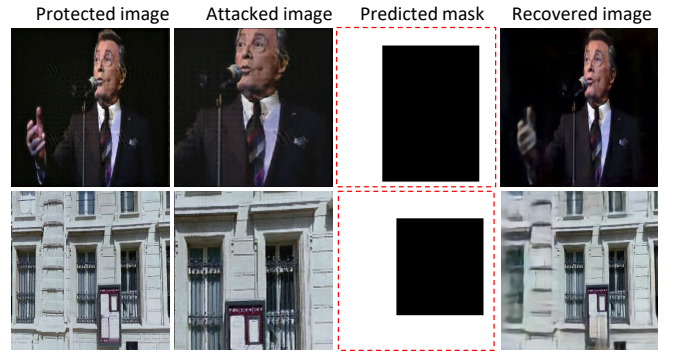


Fig. 1. Illustration of the functionality of CLR-Net. We embed imperceptible perturbations to transform images into the protected images. Malicious attacker deliberately crops the two images to mislead the audience. CLR-Net localizes the cropped region and successfully recovers the image.

Cropping is the process of removing unwanted areas of an image. It enlarges the subjects inside the preserved areas, which improves the magnification of a photograph, creates focus and strengthens the composition [138]. However, cropping can also be an extremely cheap and effective way to maliciously alter the underlying meaning. Fig. 1 shows two examples of malicious image cropping forgery. The attackers crop the images and mislead the audience with fake comments. Without the ground truth as a reference, people are easily deceived by what they observe from the manipulated images. What's worse, they might further circulate these fake images. As a result, fabricating stories by cropping can be a means for some politicians to influence public opinion.

Sadly, image cropping forgery detection [44], [61], [65], [66], [84], is still an ill-posed problem. There are few previous arts for image crop forgery detection. The overwhelming majority focuses on crop detection instead. Compared to traditional image splicing or copy-paste detection [56], [88], [99], crop forgery detection is much less investigated. Most previous schemes for image cropping forgery detection only focus on predicting whether the image is cropped by searching for traces that expose image crops. There are fewer image cropping localization schemes [66], [84]. Besides, these methods have certain limitations that make them applicable only to a subset of images. For example, [66] requires the images to be untouched and uncompressed so that tiny traces like chromatic aberration and vignetting exist. In [84], a watermark for cropping localization must be shared with the

recipient. These constraints are hard to be satisfied in the real world. Besides, there are plenty of photo cropping applications that turn image cropping into hybrid attacks. One may also subsequently resize, compress or even blur the cropped image to conceal his behavior. The main difficulty for image cropping detection is mainly that the remaining image fragment cannot provide enough universal trace to reveal the behavior. The existing crop detection algorithms [61], [65] mainly focus on predicting whether an image is cropped. They are represented by detecting the exposing evidences of asymmetrical image cropping. However, cropping different areas within the same image will result in different semantic changes, and therefore we need to locate the position of the crop in the original image plane. Apart from the existing drawbacks, we argue that even a successful cropping prediction or localization is not enough. Cropping-out different areas of an image usually leads to drastically varied intentions. For example, how to distinguish benign cropping behaviors from those malicious attacks, such as discarding a visible watermark or removing a person? Therefore, we are motivated to develop a scheme that recovers the entire image from the cropped fragment, despite the presence of real-world image processing., e.g., JPEG compression, Gaussian blurring, etc.

Watermarking [13], [69], [81] aims at hiding information imperceptibly into the host data for covert purposes. The technology focuses on robustness against possible digital attacks, such as image compression, noise adding, filtering, etc. Watermarking has been widely used in copyright protection and content authentication of images in multimedia. Recently, many novel watermarking schemes for image protection is proposed. Khachaturov et al. [33] propose a watermarking-like adversarial method that prevents inpainting systems to perform normally on a protected image. In [34], the authors propose an adversarial attack method to cause errors in super-resolution model, making the generated image contain undesired style. The myth behind these schemes is that once the secret information successfully travels through online social networks, the recipient can decode the information to administrate a number of covert tasks.

This paper explores the potential of robust watermarking on image cropping localization and recovery. We propose a novel robust watermarking network for image Cropping Localization and Recovery (CLR-Net). When a targeted image is cropped, CLR-Net simultaneously localizes the cropped region and recovers the entire image. We propose a generator based on Invertible Neural Network (INN) [72] to transform an original image into its protected version. The difference before and after image protection is close to imperceptible. Afterwards, we use an attacking layer to simulate malicious crop and benign image processing attacks. On the recipient's side, we pre-process the attacked image using a Siamese network [106]. Then, a localizer is proposed to estimate the cropping mask and a confidence score. We rectify the image according to the cropping mask by resizing and zero-padding. The inverse process of the generator recovers the original image. For enhanced robustness of CLR-Net in real-world applications, we innovatively propose a novel Fine-Grained generative JPEG simulator (FG-JPEG). Besides the traditional

agenda of iterative training with the attack layer, a Siamese network is proposed for image pre-processing on the attacked images where we minimize the performance gap against two different attacks in each iteration.

Comprehensive real-world experiments demonstrate that CLR-Net accurately estimates the cropping mask and recovers the full image even if the attacker processes the cropped image. The extensive ablation studies also prove the necessity of the network design as well as the training strategies.

The main contributions of this paper are three-folded.

- We propose the first scheme for image cropping localization and recovery based on robust watermarking.
- Imperceptibility of the watermark embedding, high quality of the recovered images and high accuracy of cropping localization can be simultaneously ensured by CLR-Net.
- We propose a fine-grained generative JPEG simulator (FG-JPEG) as well as an image pre-processor based on a Siamese network architecture that noticeably improves the real-world robustness of CLR-Net.

II. RELATED WORKS

In this section, we review the related works of the proposed method, namely, image watermarking, image cropping detection & localization, and invertible networks for data hiding.

A. Image watermarking

Watermarking [1], [112], [139] is an important branch of steganography [140], [141] which highlights robust and imperceptible information hiding into the host data for covert purposes. Many traditional image watermarking methods work on different transform domains including Discrete Fourier Transform (DFT) [110], Discrete Cosine Transform (DCT) [111], [116], Discrete Wavelet Transform (DWT) [114], [115] and Dual-Tree Complex Wavelet Transform (DTCWT) [81], [113]. With the emergence of deep learning, there exists a number of deep-network-based watermarking methods [13], [36], [82]. An encoder is usually employed to transform the original images into marked images, and a decoder extracts hidden message from the received image. To enable robustness, these schemes usually follow a multi-task learning agenda where in each iteration the algorithms add a selected kind of attack on the marked images. The attacks are implemented by an attack layer using differentiable methods. However, different image post-processing attacks share varied characteristics, and such technique can potentially lead to unbalanced robustness.

Many fragile watermarking schemes for image self-recovery have been proposed. He et al. [48] embed the shuffled DCT coefficients into the Least Significant Bit (LSB) planes of the host image. As a result, after data extraction by the recipient, he can only recover a blurry version of the original image. Zhang et al. [25] propose to embed into the image blocks check-bits and reference-bits, where the former identify the tampered blocks and the latter can exactly reconstruct the original image. Korus et al. [51] theoretically analyze the reconstruction performance with the use of communication theory. But these methods are fragile and not developed for image cropping recovery. Our previous work named Imuge [35]

presents a robust watermarking scheme that protects images from being maliciously manipulated. After the recipient gets the tampered protected image, he can conduct accurate tamper localization and image recovery. What's more, there are some works that uses watermarking for the prevention of image inpainting [33] or super-resolution (SR) [34].

However, none of the above-mentioned works address the issue of image anti-cropping using image cropping recovery. This paper addresses the issue of robust image cropping localization and recovery.

B. Image cropping detection and localization.

The existing image cropping detection algorithms [44], [61], [65] mainly focus on predicting whether an image is cropped. They are represented by detecting the exposing evidences of asymmetrical image cropping, e.g., the shift of the image center [65], and the inconsistency of JPEG blocking artifacts [44], [61]. Fanfani et al. [65] propose an automated approach for detecting asymmetrically cropped images, where the shift of the image center with respect to the principal point is used to assess cropping. Yerushalmy et al. [61] exploit image artifacts that are due to chromatic aberrations as indicators for evaluating image authenticity. The trace is introduced in the acquired image by the optical and sensing systems of the camera. Specifically, in [44], the block artifact grids (BAGs) are extracted blindly with a new extraction algorithm, and then abnormal BAGs can be detected with a marking procedure as a trail of cropping detection. In comparison, there are fewer schemes developed for image cropping localization. Van et al. [66] investigate the subtle traces that cropping has on the image distribution, and predicts the absolute location of image patches. For example, lenses will leave behind certain clues, notably chromatic aberration and vignetting. We previously present a robust watermarking scheme for image cropping localization [84]. The image owner embeds a selected watermark and the recipient can robustly extract the watermark and conduct feature matching to predict the cropping mask.

However, there are certain issues to be addressed. Van et al. [66] require the images to be untouched and uncompressed so that the tiny clues are preserved. Otherwise, the scheme cannot find enough trace for cropping localization. For [84], the watermark must be shared with the legal recipient. In contrast, we present CLR-Net that localizes image cropping and conducts image recovery using robust watermarking. It does not require a shared image as the watermark and has no restriction on the image format or quality.

C. Invertible networks for data hiding

Invertible neural network (INN) learns a stable invertible mapping from the source distribution \mathcal{P}_s to a targeted distribution \mathcal{P}_t , and the forward and back propagation operations are in the same network. Pioneering research on INN-based mapping can be seen in NICE [70] and RealNVP [71]. Previously, INNs are successfully applied for various low-level computer vision tasks, e.g., image colorization [73], image rescaling [74], etc. Most recently, Lu et al. [77] and Jing et al. [103] both use invertible neural networks based on RealNVP for data

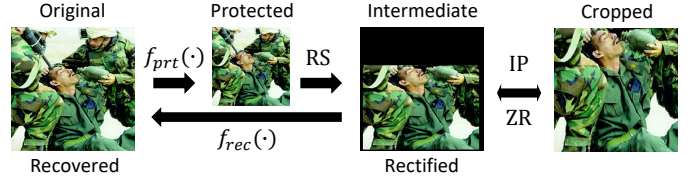


Fig. 2. **Problem statement of CLR-Net.** We decompose image cropping into several steps and build invertible functions for image cropping recovery. RS, IP, ZR respectively denotes *region selection*, *image post-processing* and *zero-padding & resizing*. Cropping localization is omitted for simplicity.

hiding and extraction. These works can largely increase the overall payload by hiding multiple images simultaneously. Xu et al. [119] make the first attempt to robustly hide multiple images into a single container using INN.

III. METHOD

We first state the problem of image cropping localization and recovery, and then introduce the network modeling accordingly. Training details and the objective loss functions of CLR-Net are also specified. Fig. 2 illustrates the problem statement of CLR-Net. The sketch of our modeling framework is presented in Fig. 3.

A. Problem statement

Ideal image cropping localization and recovery. We begin with decomposing image cropping manipulation into several independent steps by Eq. (1).

$$\mathbf{X}_{atk} = IP(RS(\mathbf{X}, \mathbf{M})), \quad (1)$$

where \mathbf{X} and \mathbf{X}_{atk} respectively denote a targeted image and its attacked version. \mathbf{M} denotes the cropping mask, which generally represents the Region of Interest (RoI) within the image. The target of image cropping localization and content recovery is respectively to estimate the cropping mask \mathbf{M} and to reconstruct the whole image \mathbf{X} . In Eq. (1), $RS(\cdot)$ denotes *region selection* that discards the information outside the selected RoI. $IP(\cdot)$ denotes *image post-processing* that truncates the image and post-processes the rest of the image using JPEG compression, Gaussian blurring, etc. Usually, an additional image resizing is involved that transforms the attacked image into an arbitrary size.

We employ two functions $f_M(\cdot)$, $f_{rec}(\cdot)$ respectively for cropping localization and content recovery.

$$\hat{\mathbf{I}} = f_{rec}\left(ZR\left(\mathbf{X}_{atk}, \hat{\mathbf{M}}\right)\right), \quad (2)$$

$$\hat{\mathbf{M}} = f_M(\mathbf{X}_{atk}), \quad (3)$$

where $\hat{\mathbf{M}}$ and $\hat{\mathbf{I}}$ are respectively the estimated cropping mask and the reconstructed image. $ZR(\cdot)$ denotes *zero-padding and reshaping* that first zero-pads the attacked image according to the estimated cropping mask and then resizes the padded image into the original size. Note that the attacker can arbitrarily reshape the image, and previous work [105] can only infer the original size approximately but not accurately. Therefore, we hypothesize that the original sizes of the images are fixed

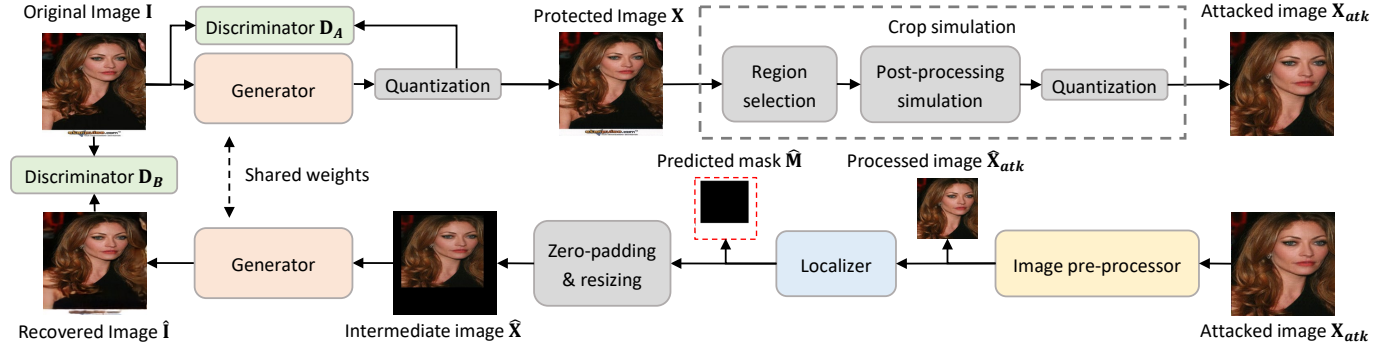


Fig. 3. **Approach overview of CLR-Net.** The generator transforms the original image into the protected image. The attack layer simulates image cropping and image processing attacks with a novel FG-JPEG. The attacked image is then pre-processed on the recipient's side, and the localizer predicts the cropping mask. We rectify the processed image by scaling and zero-padding. Finally, the inverse process of the generator estimates the original image.

or specified by the recipient. If the cropping localization is correct, $ZR(\cdot)$ is the inversion of $RS(\cdot)$.

Dealing with inadequate information. Modeling Eq. (2) is ill-posed. For natural images, though adjacent pixels usually share some spatial correlation, it is empirically impossible for the attacked image to contain any information of the cropped-out contents. Thus, directly solving Eq. (2) will lead to sub-optimal solutions where the destroyed contents are hallucinated by the networks. To address this issue, we employ a third function $f_{prt}(\cdot)$ to embed deep representations of an original image, denoted as \mathbf{I} , into itself, and let $\mathbf{X} = f_{prt}(\mathbf{I})$ in Eq. (1). Accordingly, Eq. (1), Eq. (2) and Eq. (3) are jointly reformulated as a pair of invertible image embedding and recovery functions, where $\mathbf{X} = f_{prt}(\mathbf{I})$ and $\hat{\mathbf{I}} = f_{rec}(\mathbf{Z}R(\mathbf{X}_{atk}, \hat{\mathbf{M}}))$. We expect that $\mathbf{X} \approx \mathbf{I}$, $\hat{\mathbf{I}} \approx \mathbf{I}$ and $\hat{\mathbf{M}} \approx \mathbf{M}$. Literally, the invertible function is to find a way of image protection against image cropping, so that even if \mathbf{X} is attacked with randomized $IP(\cdot)$ and $RS(\cdot)$, we can correspondingly predict \mathbf{M} and estimate the original \mathbf{I} .

Then, we start to model the problem using hybrid neural networks and heuristic functions. First, given the invertible nature of the problem, we can employ an INN-based generator \mathbf{G} to learn $f_{prt}(\cdot)$ in the forward pass and $f_{rec}(\cdot)$ in the backward pass. Since we will not be informed of the original size of the image, the intermediate image $\hat{\mathbf{X}}$ needs to be loaded with a fixed size by the generator. Next, $f_M(\cdot)$ can be learnt by another network named localizer \mathbf{C} , and the attacked image \mathbf{X}_{atk} can be heuristically rectified by a function $ZR(\cdot)$. Third, to enable robustness training, we can follow the popular way of including an attack layer \mathbf{A} to simulate the image redistribution stages. The layer includes $RS(\cdot)$ and $IP(\cdot)$. Finally, two discriminators \mathbf{D}_A and \mathbf{D}_B can be introduced to respectively improve the quality of \mathbf{X} and $\hat{\mathbf{I}}$ by distinguishing them from the original images.

Issues on robustness training. Before implementing the functions, we further post two critical issues on improving the robustness training.

The first issue is the adaptiveness of JPEG simulation. Previous researches have proposed several mask-based JPEG simulator [13], [36], [82] by step-by-step simulation using differentiable methods. However, the hand-crafted quantization

tables in these schemes are immutable, which is in contrast with the quantization table in real-world JPEG images that can be customized and adaptively controlled by the quality factor as well as the image content. As a result, the neural networks can overfit and lack real-world robustness. To address this, we tempt to add more flexibility in JPEG simulation by proposing the novel generative FG-JPEG simulator.

The second issue is that we need to consider that $IP(\cdot)$ is likely to contain a large solution space in the real world. Different image post-processing attacks share varied characteristics, such as randomized addition or removal of higher-band information. However, the traditional way of using an attacking layer only provides multi-task guidance, which cannot explicitly circumvent uneven network performance against different kinds and strengths of attacks. To address this, we extend the pipeline by pre-processing the received \mathbf{X}_{atk} into a processed version $\hat{\mathbf{X}}_{atk}$ ahead of cropping localization and recovery. Given attacked versions of a same protected image, a Siamese network is used to transform these copies by minimizing their mutual differences. The purpose is to help the subsequent network identify and utilize the features most tolerant to all possible digital image post-processing attacks for information embedding and image recovery.

B. Pipeline design

Image protection. Given the original image \mathbf{I} , we generate the protected image \mathbf{X} using the forward pass of \mathbf{G} . Then, \mathbf{I} can be held secret and we share \mathbf{X} on the social network instead. We propose an invertible U-shaped network similar to [74]. According to Fig. 3, the network is composed of three stacked downscaling modules and three upsampling modules. Each module contains a Haar downsampling or upsampling transformation layer and four double-sided affine coupling layers. The wavelet-based blocks provide empirical biases to decompose the features into the lower-band and higher-band information, where the latter is essential for image protection and recovery. We apply Spectral Normalization (SN) [83] in each block in that SN helps stabilize the training by restricting the Lipschitz constant of the network within one.

Cropping simulation. We utilize an attack layer \mathbf{A} to implement *region selection* and *image post-processing* in the

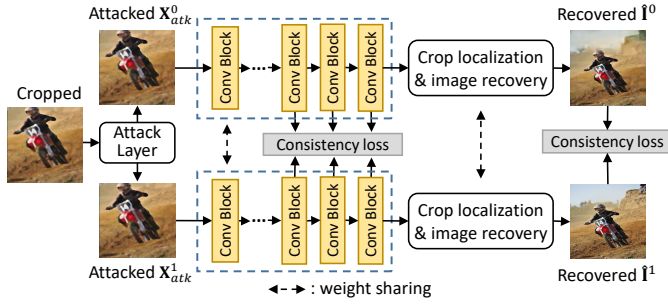


Fig. 4. **The Siamese architecture of the image pre-processor.** The attack layer generates two attacked views of the cropped image using arbitrarily-sampled attacks. The Siamese network processes the images using shared weights. We minimize the consistency loss between the image features as well as the performance gap under the two attacks.

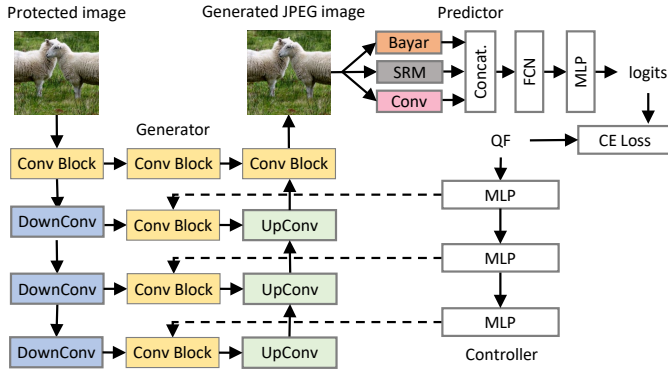


Fig. 5. **Network architecture of FG-JPEG.** The generator takes the protected image and simulates the JPEG compression, which is conditioned by the controller. The predictor classifies the QF of the generated images.

real-world application. First, we use a differentiable image quantization method [101] to convert the floating-point values of \mathbf{X} to 8-bit integer. Then, we freely generate cropping masks \mathbf{M} to crop the protected images. The survival rate is set as $r_c \in [0.5^2, 1^2]$, where 0.5^2 stands for preserving only 25% squared-size area of \mathbf{X} while the rest are cropped. Afterwards, we resize the cropped image and simulate common image post-processing attacks using classical differentiable methods [13]. The attacks include the following: (1) *resizing*: we resize the image by an arbitrarily resizing rate $r \in [50\%, 150\%]$, (2) *median blurring*, we blur the image using median filter whose kernel size k is arbitrary selected from 3, 5, (3) *Additive White Gaussian Noise (AWGN)*, which adds Gaussian noise evenly on the image, where the standard value s ranges from zero to one. (4) *Gaussian blurring*, which is similar to the median blurring but the kernel is different. (5) *JPEG compression*. We exceptionally apply our own FG-JPEG to produce high-fidelity JPEG images with controllable quality factor. The design of FG-JPEG is specified in Section III-C. The considered quality factor ranges from [50, 100]. Afterwards, \mathbf{X}_{atk} is again quantized into the 8-bit integer format.

Image pre-processor. Fig. 4 illustrates the architecture of the image pre-processor, which transforms the attacked images into a more clustered distribution. During training, the Siamese networks process two different images using the same network. The attack layer arbitrarily selects two kinds of image post-

processing attacks and generates two corresponding attacked images \mathbf{X}_{atk}^0 and \mathbf{X}_{atk}^1 from a same \mathbf{X} . On cropping \mathbf{X}_{atk}^0 , \mathbf{X}_{atk}^1 , we use a shared mask \mathbf{M} in each iteration. Afterwards, we respectively conduct cropping localization and image recovery based on the two views, where the estimated masks as well as the recovered images are respectively denoted as $\{\hat{\mathbf{M}}^0, \hat{\mathbf{I}}^0\}$, $\{\hat{\mathbf{M}}^1, \hat{\mathbf{I}}^1\}$. We restrict that the generated feature representations as well as the performance of CLR-Net against the two attacks should be close between each pair. More details are specified in the introduction of loss function (Section III-E).

The Siamese network is built upon a simple six-layered FCN architecture. Each *Conv* block within the FCN shown in Fig. 4 consists of a *Conv* layer, an ELU activation layer and an Instance Normalization (IN) layer.

Cropping localization. After image pre-processing, the localizer \mathbf{C} estimates the cropping mask $\hat{\mathbf{M}}$ and the confidence score S . The network is built upon a three-layered lightweight U-Net network that transforms $\hat{\mathbf{X}}_{atk}$ into a one-dimensional feature. The feature is then flattened and fed into a four-layered Multi Layered Perceptron (MLP). The output of the MLP is $\{x_0, y_0, x_1, y_1, S\}$, where $\{x_0, y_0, x_1, y_1\}$ represents the coordinates of the upper-left and lower-right corner of the rectangle-shaped $\hat{\mathbf{M}}$. \mathbf{X}_{atk} is detected as *cropped* if $S \geq 0.5$. We also feed \mathbf{C} with original images \mathbf{I} and expect the corresponding score S to be close to zero. It lowers the false alarm rate of CLR-Net.

Zero-padding and resizing. We resize and zero-pad $\hat{\mathbf{X}}_{atk}$ according to the estimated cropping mask. The intermediate image $\hat{\mathbf{X}}$ places the preserved contents in the correct location with the cropped-out contents left blank.

Estimating the original image. After zero-padding and resizing, we send $\hat{\mathbf{X}}$ into the generator \mathbf{G} and inversely run the network to estimate the original image \mathbf{I} .

Adversarial training. The two discriminators \mathbf{D}_A and \mathbf{D}_B are built upon the popular Patch-GAN [18]. They facilitate the imperceptibility of the watermark embedding and the overall quality of the generated images.

C. Fine-grained generative JPEG simulator

We propose a generative JPEG simulator called FG-JPEG to transform plain-text images into simulated JPEG images. FG-JPEG needs to be trained ahead of the pipeline with paired $\{\mathbf{I}, \mathbf{I}_{jpg}\}$, where \mathbf{I}_{jpg} are the real-world JPEG images generated in advance. FG-JPEG consists of a generator, a controller and a predictor. Fig. 5 illustrates the network design. The predictor classifies the quality factor of a target image. It is trained by estimating the QF of real-world JPEG images. We train the predictor ahead of the generator and the controller. The network is implemented by a light-weight ResNet-32 architecture. Since the differences between JPEG images and plain-text images lie mainly in the higher frequents, we replace the leading *Conv* layer with a vanilla *Conv* layer, a SRM *Conv* layer [96] and a Bayar *Conv* layer [97] in parallel. The introduction of SRM *Conv* and Bayar *Conv* is to augment details of the images, since JPEG compression generally alters the higher-frequent details and keeps intact the semantic information. For QF classification, the QF labels

are set as $QF \in \{10, 30, 50, 70, 90, 100\}$ to ensure that the discrepancy among adjacent categories is significant enough for classification. Besides the generator, the JPEG controller is to control the generation of simulated JPEG images, while the predictor is to estimate whether the QF classification result of the output image can match that of the real-world JPEG image with the same QF. The estimated quality factor can be changed with interactive selections to have a balance between artifacts removal and details preservation. The generator is built upon the popular four-leveled U-Net architecture. In each level, there is a pair of a down-sampling block, an up-sampling block, and a channel-wise concatenation in between as a shortcut. Traditional U-Net-based networks consist of an encoder part, a decoder part, a *Conv* block linking the two parts and channel-wise concatenations in between the different levels as shortcuts. We introduce an additional convolutional block to replace the straightforward concatenation in each level. The implementation of the *Conv* blocks is identical to those in the image pre-processor, and we use bilinear interpolation to conduct rescaling in the down-sampling and up-sampling blocks. Furthermore, we let the output of the lower three levels of the additional *Conv* blocks be conditioned on the output of the controller. The controller is a six-layered MLP. The network is provided with a targeted quality factor $QF \in [0, 100]$, and the first three layers transform $QF/100$ into deep features. Inspired by Adaptive Instance Normalization (AdaIN) [145], we let the last three layers learn the mapping functions that output modulation parameter pairs a, b that control the standard deviation and mean of the features.

$$\mathbf{F}_{out,i} = a_i \cdot \text{Conv}(\mathbf{F}_{in,i}) + b_i, \quad (4)$$

where \mathbf{F}_{in}^i and \mathbf{F}_{out}^i respectively denote the input and output features of the additional convolutional block at i_{th} level. After the generation of $\hat{\mathbf{I}}_{jpg}$, the predictor provides classification results \hat{QF} on $\hat{\mathbf{I}}_{jpg}$, and the results should be close with those of \mathbf{I}_{jpg} with QF . When we apply FG-JPEG in the pipeline of CLR-Net, we consider that the difference of \mathbf{I} and \mathbf{X} lies mainly in the higher bands. Accordingly, we additionally introduce some Additive White Gaussian Noise (AWGN) on \mathbf{I} and encourage the removal of higher-band details including AWGN during training FG-JPEG. We set $\delta_{QF} = 20$ among the neighboring categories where the discrepancy can be significant enough for classification. We allow the network to give an imprecise estimation when QF lies in between two neighboring categories.

D. Tamper-based data augmentation

Apart from the pipeline design, we consider minimizing the impact of spatial correlation within natural images on the image cropping recovery process. Previously, many image restoration schemes rely heavily on the deep image prior (DIP) [87]. Therefore, deep networks can easily find the shortcut that image recovery is easy in most cases simply with the help of DIP. As a result, image protection is largely ignored in the forward pass by hallucinating the results in the way image out-painting does. However, in real-world image cropping, objects are prone to being entirely cropped out, where DIP provides

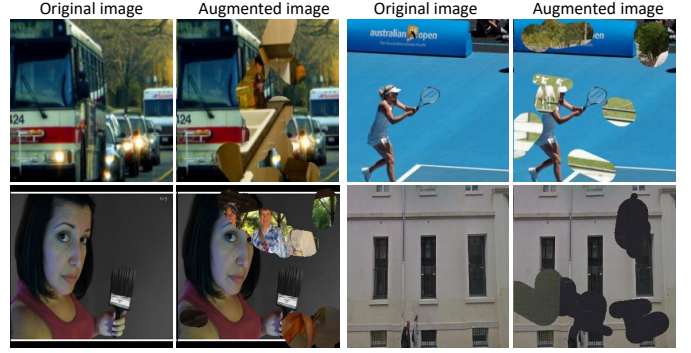


Fig. 6. **Example of tampering-based data augmentation.** We deliberately tamper the original images by arbitrarily adding irrelevant contents. It reduces the pixel redundancy within natural images.

no clue for their recovery. Therefore, how to guide the network to correctly estimate the image without using the image prior is a big issue for CLR-Net.

We propose a tailored and novel data augmentation that applies image manipulation as image pre-processing. Our experiments show that simply varying the generated cropping mask is not enough to evade such *shortcut learning* [26], as in many cases they are not adaptive enough to cover the Regions of Interests (ROIs) within each image. Therefore, it requires extra efforts to disable the network from relying on the natural intrinsic of DIP. Fig. 6 shows two examples of our tamper-based data augmentation. The methodology is simple yet effective, where we deliberately and arbitrarily introduce some unrelated contents on a portion r_{aug} of the original training set. A number of random areas within the original image \mathbf{I} are selected and manipulated according to a tampering mask \mathbf{M}_t . The augmented image \mathbf{I}_{aug} is generated as, $\mathbf{X}_{tmp} = \mathbf{I} \cdot (1 - \mathbf{M}_t) + \mathbf{R} \cdot \mathbf{M}_t$, where \mathbf{R} denotes irrelevant contents borrowed from other images. We use the free-form mask generation algorithm proposed in DeepFillV2 [85] to generation \mathbf{M}_t , where the number of strokes and length of the tampering are all controllable. When the added contents are cropped out, the only possible way for successful recovery is to hide information during image protection. We empirically find that $r_{aug} = 15\%$ provides the best performance. The reason is that while DIP is not reliable for image recovery, it can still facilitate efficient encoding of image representation.

E. Objective functions

The objective functions include the protection loss \mathcal{L}_{prt} , the cropping localization loss \mathcal{L}_{loc} , the recovery loss \mathcal{L}_{rec} , the consistency loss \mathcal{L}_{cons} and the adversarial losses \mathcal{L}_{adv}^{DA} and \mathcal{L}_{adv}^{DB} . There is also the JPEG simulation loss \mathcal{L}_{jpg} for FG-JPEG. In the below equations, $\alpha, \beta, \gamma, \theta, \eta$ are hyper-parameters.

Generator. The protection loss \mathcal{L}_{prt} and the recovery loss \mathcal{L}_{rec} respectively encourage \mathbf{X} and $\hat{\mathbf{I}}$ to resemble \mathbf{I} . We use the popular ℓ_1 loss term to measure the distance between images.

$$\mathcal{L}_{prt} = \|\mathbf{I} - \mathbf{X}\|_1, \quad (5)$$

$$\mathcal{L}_{rec} = \|\mathbf{I} - \hat{\mathbf{I}}\|_1. \quad (6)$$

Discriminator. For adversarial training, the discriminators \mathbf{D}_A and \mathbf{D}_B need to respectively distinguish \mathbf{X} and $\hat{\mathbf{I}}$ from \mathbf{I} . The adversarial loss \mathcal{L}_{adv} for the main pipeline is as follows.

$$\mathcal{L}_{adv} = \log(1 - \mathbf{D}_A(\hat{\mathbf{X}})) + \log(1 - \mathbf{D}_B(\hat{\mathbf{I}})). \quad (7)$$

The loss for the two discriminators are respectively

$$\mathcal{L}_{D_A} = -\frac{1}{2}(\log \mathbf{D}_A(\mathbf{I}) + \log(1 - \mathbf{D}_A(\hat{\mathbf{X}}))), \quad (8)$$

$$\mathcal{L}_{D_B} = -\frac{1}{2}(\log \mathbf{D}_B(\mathbf{I}) + \log(1 - \mathbf{D}_B(\hat{\mathbf{I}}))). \quad (9)$$

Localizer. The localization loss \mathcal{L}_{loc} is to minimize the binary cross entropy (BCE) loss between $\hat{\mathbf{M}}$ and \mathbf{M} . In Eq.(10), H and W denote the width and height of the image.

$$\mathcal{L}_{loc} = -\frac{1}{HW} \sum (\mathbf{M}_{i,j} \log \hat{\mathbf{M}}_{i,j} + (1 - \mathbf{M}_{i,j}) \log(1 - \hat{\mathbf{M}}_{i,j})). \quad (10)$$

Image pre-processor. For the Siamese network, we introduce the consistency loss that prevents biased performances against different attacks. Our target is that in each training iteration, $\hat{\mathbf{M}}^0 \approx \hat{\mathbf{M}}^1$, $\hat{\mathbf{I}}^0 \approx \hat{\mathbf{I}}^1$. Besides, we also minimize the generated deep representations ϕ_n^0 , ϕ_n^1 of the two images by including the consistency loss. Third, we prevent the Siamese network from drastically changing the image. Therefore, the consistency loss is:

$$\mathcal{L}_{cons} = \sum_{n \in [3,5]} \|\phi_n^0 - \phi_n^1\|_1 + \|\hat{\mathbf{M}}^0 - \hat{\mathbf{M}}^1\|_1 + \|\hat{\mathbf{I}}^0 - \hat{\mathbf{I}}^1\|_1 + \|\hat{\mathbf{M}}^0 - \mathbf{I}\|_1, \quad (11)$$

where $n \in [3, 5]$ indicates that we compare the deep representations from the third to fifth layer of the Siamese network.

Total loss for image protection pipeline. The total loss for CLR-Net is based on the processed image provided by \mathbf{P}_{stu} .

$$\mathcal{L} = \mathcal{L}_{prt} + \alpha \cdot \mathcal{L}_{rec} + \beta \cdot \mathcal{L}_{loc} + \gamma \cdot \mathcal{L}_{cons} + \eta \cdot (\mathbf{D}_A + \mathbf{D}_B). \quad (12)$$

FG-JPEG. The generative JPEG simulator is trained ahead of CLR-Net. We use the Cross-Entropy (CE) loss to train the JPEG predictor.

$$\mathcal{L}_{QF} = CE(\mathbf{Q}_o, \mathbf{Q}_r) = -\sum_{c=1}^6 y_{o,c} \log(p_{o,c}), \quad (13)$$

where $y_{o,c}$ is the binary indicator if class label c is the correct classification for observation o . $p_{o,c}$ is the estimated probability observation o is of class c . \mathbf{Q}_o takes the $\arg\max$ of o that maximizes p . The JPEG generator and controller are jointly optimized by minimizing:

$$\mathcal{L}_{jpg} = \|\mathbf{I}_{jpg} - \hat{\mathbf{I}}_{jpg}\|_1 + \epsilon \cdot CE(\mathbf{QF}, \hat{\mathbf{QF}}). \quad (14)$$

F. Training details

Hyper parameters. The hyper-parameters are set as $\alpha = 1.5$, $\beta = 0.1$, $\gamma = 0.05$, $\epsilon = 0.1$ and $\eta = 0.01$. To better control the quality of the protected image, we additionally regulate that if the average PSNR between the original and protected image is lower than an expected threshold, e.g., 32.5dB, we let $\alpha = 4$, which encourages lower magnitude of embedding. The computational complexity of CLR-Net is comparatively low.

The networks are in sum composed of 7.84 million trainable parameters. We train CLR-Net on two Nvidia RTX 3090 GPUs and in each second CLR-Net can infer 8.63 images during testing. The batch size of CLR-Net during training is set as 4. We use Adam optimizer [40] with the default parameters. The learning rate is 1×10^{-4} with cosine annealing decay. In the following, we clarify the essential training details of CLR-Net. **Multi-staged training and synchronization.** Directly training CLR-Net with heavy image post-processing attacks from the beginning is with great difficulty featured by gradient explosion. Besides, content recovery can only be conducted after successful image cropping localization, i.e. if cropping localization fails, the wrongly estimated cropping mask will mislead the generator. Such failure of precise cropping mask estimation always happens at the early training stage of CLR-Net that prevents the networks from being stably trained.

To alleviate these issues, we introduce two effective tricks during training, namely, detaching the student network and task decomposition. At the early stage, we let the generator be updated based on the supervision loss of the teacher network, where we directly feed \mathbf{P}_{tea} with the cropped image, i.e., at this stage, the main stream is trained without the presence of image processing attacks. Meanwhile, the student network is trained in parallel with the main stream, but we attack the cropped image and feed \mathbf{P}_{stu} with the detached version of the attacked image. The supervision loss of \mathbf{P}_{stu} is only used to update \mathbf{P}_{stu} itself. We monitor the consistency loss \mathcal{L}_{feat} that compares the features from the last three blocks of \mathbf{P}_{stu} with those from \mathbf{P}_{tea} . When \mathcal{L}_{feat} is lower than a threshold $Th = 0.001$, we end the stage and block the gradient flow from \mathbf{P}_{tea} where \mathcal{L}_{tea} is then only used for updating \mathbf{P}_{tea} . Afterwards, the main stream is always jointly trained with \mathbf{P}_{stu} .

The task-decomposition strategy is similar to that in Imuge [35]. At the early stage of training, we feed CLR-Net with the ideal intermediate image $\hat{\mathbf{X}}^{id}$ for image recovery. The localizer \mathbf{C} is trained in parallel, but the unreliable output $\hat{\mathbf{M}}$ is not fed into \mathbf{G} . When the localization loss gradually converges, we combine the two tasks and therefore $\hat{\mathbf{I}}$ is generated according to $\hat{\mathbf{M}}$. In the later stage, \mathbf{G} can adapt to the possible small inconsistency between the ideal \mathbf{M} and $\hat{\mathbf{M}}$. Furthermore, we propose to automatically adjust the ground truth for the recovered image. We calculate the affine transformation function $Aff(\cdot)$ where $\hat{\mathbf{M}} = Aff(\mathbf{M})$. Then the ground truth for the recovered image is also shifted according to $Aff(\cdot)$. It alleviates the negative impact of biased cropping localization on image recovery during training.

Stabilizing the gradient. There is the potential risk of gradient explosion or vanishing since in our pipeline, the data owner's side is chained with the attack simulation as well as the recipient's side. Inspired by Zhang et al. [109] that the backward process of the attacking layer might not influence the pipeline performance too much, we propose to block the unnecessary back-propagation of the gradient flow into the attack layer as well as the image pre-processor. We calculate the difference $\delta = \hat{\mathbf{X}}_{atk} - \mathbf{X}$, where we clone and detach $\hat{\mathbf{X}}$ to cut the gradient flow. Then $\hat{\mathbf{X}}_{atk}$ is regenerated by $\hat{\mathbf{X}}_{atk} = \delta + \mathbf{X}$. By doing so, we shorten the path for gradient descent and speed up the training process.

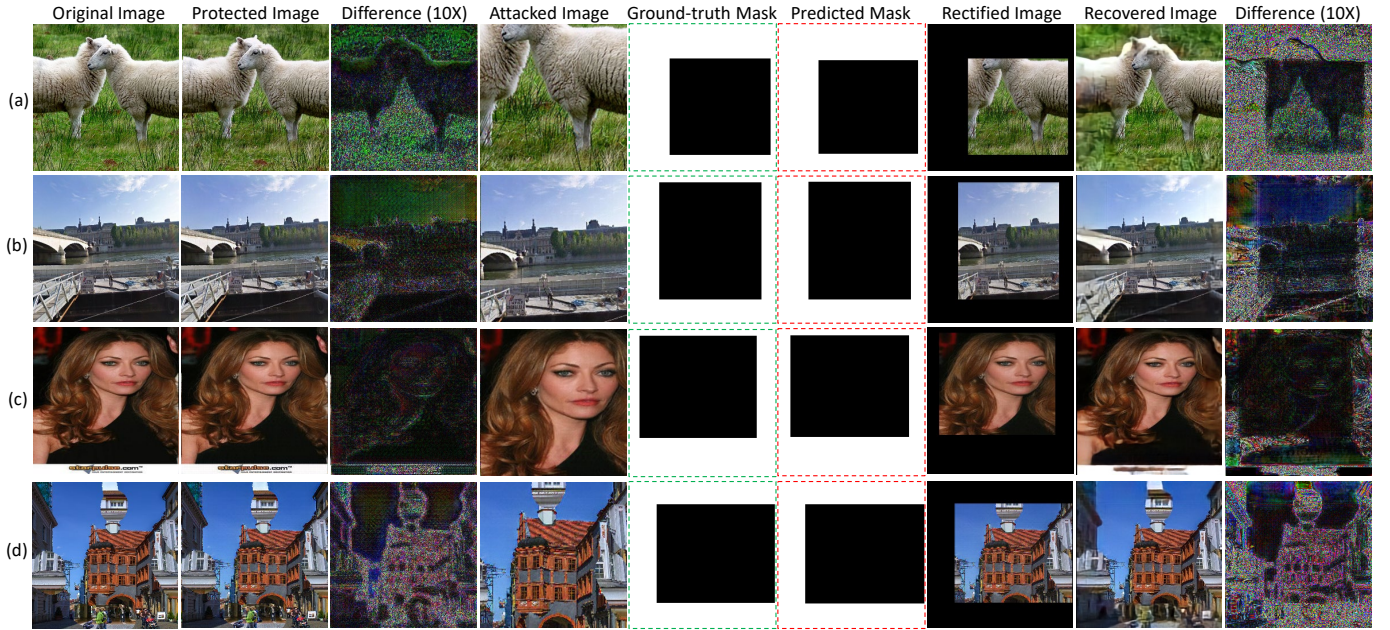


Fig. 7. **Experimental results on images from different datasets.** The involved image post-processing attacks are respectively (a) no attack, (b) JPEG compression (QF=80), (c) Median blurring (k=3) and (d) resizing (s=70%). The results of cropping localization and recovery are both satisfactory.

TABLE I
AVERAGE PSNR AND SSIM BETWEEN THE ORIGINAL AND PROTECTED IMAGES UNDER DIFFERENT RESOLUTIONS.

Dataset	512 ²		256 ²		128 ²	
	PSNR	SSIM	PSNR	SSIM	PSNR	SSIM
MS-COCO	30.13	0.927	32.67	0.933	33.52	0.943
ImageNet	30.01	0.927	33.01	0.937	33.33	0.940
UCID	29.52	0.920	32.15	0.920	33.01	0.935
Flicker	31.03	0.932	33.13	0.940	33.78	0.951

IV. EXPERIMENTS

In this section, we provide comprehensive experiments to validate the effectiveness of CLR-Net. We begin with analyzing the performance of our method. Then we compare CLR-Net with some previous arts. Also, we validate the network design via ablation studies.

A. Experimental settings

Data preparation. During training, the original images \mathbf{I} in our scheme are from a mixture of multiple popular image datasets, namely, MS-COCO [21], CelebA [93], Flickr [104], UCID [89], ImageNet [19], Places [94], Paris Street View [107] and DIV2K [90]. We arbitrarily select around 10000 images from the training set of the above datasets. We build the test set in the same way with 1000 images from each. We do not build the validation set and train the networks for 20 epochs. Unlike some previous schemes [13], [84] that train individual networks for different attacks or datasets, we train a universal model for all possible image attacks, but we train different models for varied resolutions considering that convolutions are not scale-agnostic. Thus,

CLR-Net can be applied on images with arbitrary resolution using the most suitable model. In the following experiments, we resize the images as $\mathbf{I} \in \mathbb{R}^{256 \times 256 \times 3}$, with the results under other typical resolutions reported in Table I and Table III. The scheme is tested with human-participated real-world attacks. The protected images are saved in 8-bit PNG format and the attacked images are randomly saved in JPEG, BMP or PNG format.

Evaluation metric. We employ the Peak Signal-to-Noise Ratio (PSNR), the Structural SIMilarity (SSIM) [27] to evaluate the image quality. SSIM is proposed generally based on the degradation of structural information, which shows high correlation between human visual perception and the structural similarity in plain views. We employ the F1 score to measure the accuracy of cropping localization. F1 score reports the overall precision and sensitivity of the scheme, where cropping localization can be considered as a binary classification problem, i.e., the pixels within a targeted image can be distinguished into either *original* or *cropped*.

Benchmark. There is no previous work that can simultaneously localize the cropped region and recover the entire image. We build a benchmark that trains two independent networks for a solution of Eq. (2), where image protection is not involved. We implement the image recovery network using a state-of-the-art and open-source image outpainting and harmonization network [67]. The architecture of the localizer and the experimental settings are identical to the baseline.

B. Quantitative analysis

Quality of the protected images. Fig. 7 showcases four experimental results of CLR-Net on cropping localization and image recovery. We can observe that the quality of \mathbf{I}_{prt} is satisfactory with the difference between \mathbf{I}_{prt} and \mathbf{I} almost

TABLE II
AVERAGE PERFORMANCE OF CROPPING LOCALIZATION AND IMAGE RECOVERY OVER 1000 IMAGES RESPECTIVELY FROM DIFFERENT DATASETS.

Survival rate	Dataset	Index	JPEG				Scaling			M-Blur	CE	Dropout	Identity
			QF=90	QF=70	QF=50	QF=10	150%	125%	75%				
$[0.5^2, 0.65^2]$	CelebA	F1	0.955	0.940	0.921	0.557	0.956	0.933	0.947	0.935	0.827	0.864	0.980
		PSNR	26.50	24.55	23.40	12.42	25.74	25.46	26.13	26.61	22.47	23.39	27.77
		SSIM	0.790	0.753	0.719	0.273	0.797	0.770	0.814	0.816	0.701	0.710	0.829
$[0.65^2, 0.8^2]$	MS-COCO	F1	0.968	0.970	0.951	0.588	0.963	0.970	0.956	0.941	0.912	0.920	0.986
		PSNR	27.46	27.30	22.20	13.41	26.34	24.94	25.75	26.34	23.04	25.46	30.18
		SSIM	0.866	0.854	0.707	0.324	0.801	0.767	0.769	0.755	0.731	0.789	0.891
$[0.8^2, 1.0^2]$	Flicker	F1	0.982	0.979	0.965	0.662	0.970	0.958	0.969	0.947	0.901	0.885	0.990
		PSNR	29.70	27.55	25.92	11.87	27.69	27.62	29.29	26.80	26.62	22.09	31.07
		SSIM	0.844	0.819	0.774	0.265	0.853	0.846	0.849	0.811	0.772	0.740	0.898

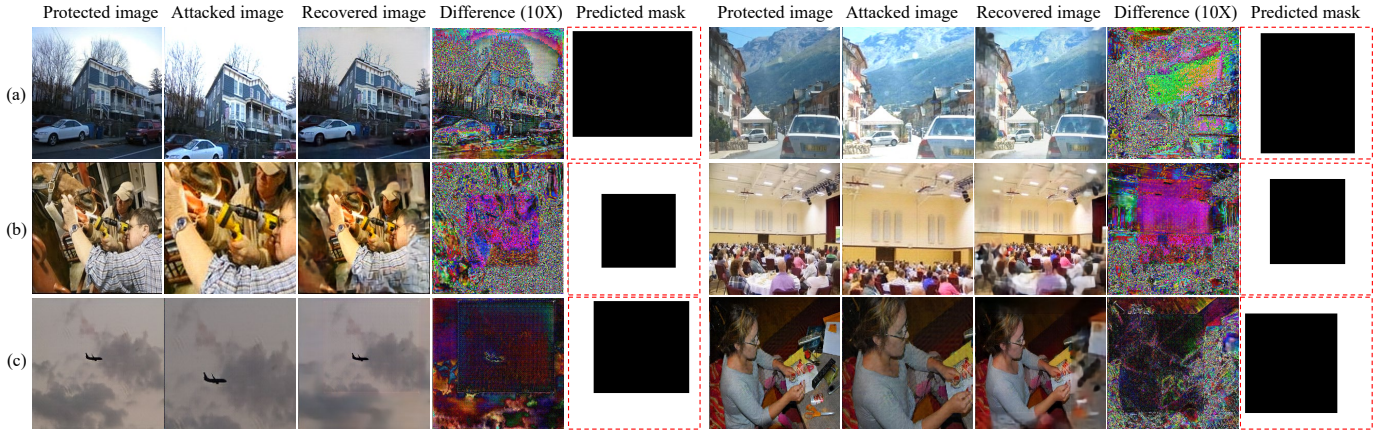


Fig. 8. **Experimental results on untrained attacks.** (a) Brightness change (+20), (b) automatic contrast enhancement using CLAHE, (c) hybrid attack (JPEG80+Resizing). We do not train the networks with brightness change, contrast enhancement since these attacks will shift the mean of the image, resulting a large variance from the ground-truth. CLR-Net manages to resist these untrained attacks in the testing stage.

imperceptible. A closer look at the augmented difference indicates that the information of the entire image is encoded in the higher bands and mainly within the image center. Also, to combat JPEG compression, we see that the embedded information are generally encoded into the chessboard style. We have conducted more embedding experiments and the results in Table I show that more perturbation is required for textured image datasets and larger images. For example, for ordinary datasets like MS-COCO, the average PSNR and SSIM are respectively 32.67dB and 0.933. UCID contains way more textured images, and the PSNR and SSIM slightly drop to 32.15dB and 0.920. Also, on MS-COCO, if the images are sized 256×256 , the averaged PSNR between the original and protected images will be close to 2.5dB higher than that of 512×512 -sized images.

Performance of cropping localization and recovery. Fig. 7 further shows the results of cropping localization and image recovery. The tests are made by the volunteers with different survival rate and image processing attacks. Because the settings of the attacks during training simulate most commonly used image post-processing attacks, we employ the same settings during testing. For example, we arbitrarily set the kernel size as three or five when we apply the Gaussian blurring attack. We can observe that the original images are recovered even with the median blurring attack and a medium-

sized cropping mask. The average PSNR between \mathbf{I} and $\hat{\mathbf{I}}$ in these cases is 26.73dB with SSIM 0.843. The cropping localization is accurate, with the average F1 score close to 0.95. Though it is not possible to predict a perfect $\hat{\mathbf{M}}$, CLR-Net learns to adapt to the trivial drift. Besides, though some details of the cropped-out contents are lost, the fidelity of the recovered contents is high in that CLR-Net does not produce them by hallucination.

We have conducted more experiments over the test set under different survival rate and benign attacks. The average performances are reported in Table II. We see that heavier attacks or larger survival rates will lower the performance of both cropping localization and recovery. For image recovery, the average PSNRs range from 23dB to 30dB. The average SSIMs are generally above 0.8, which can provide satisfying and trust-worthy recovery results.

Performance generalization on untrained attacks. In Fig. 8, we test CLR-Net on several untrained attacks, namely, brightness change, contrast enhancement and hybrid attack. For brightness change, each pixel within the image is subtracted with a same digit arbitrarily ranging from $[-20, 20]$ where the resulting overflow/underflow pixels will be clamped. For contrast enhancement, we employ the automatic Contrast Limited Adaptive Histogram Equalization (CLAHE) [117] implemented by the OpenCV library. For drop-out, the dropping-out rate is arbitrarily selected from $[0, 0.3]$. We see that the results

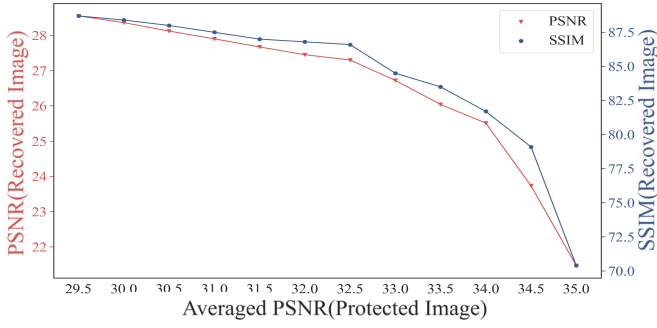


Fig. 9. Curves of averaged PSNR for protected images versus averaged PSNR/SSIM for recovered images.

TABLE III

AVERAGE PERFORMANCE OF CROPPING LOCALIZATION AND IMAGE RECOVERY ON DIFFERENT-RESOLUTIONED IMAGES FROM MS-COCO.

Size	Index	JPEG			Identity	MBlur
		QF=90	QF=70	QF=50		
512 ²	F1	0.965	0.943	0.912	0.979	0.936
	PSNR	26.67	26.20	23.46	28.11	24.15
	SSIM	0.843	0.829	0.723	0.867	0.752
128 ²	F1	0.986	0.967	0.955	0.991	0.963
	PSNR	28.26	27.63	24.85	31.30	27.01
	SSIM	0.871	0.854	0.753	0.912	0.846

are also satisfactory, where the cropped part can be effectively localized. Interestingly, the recovered contents tend to be more close to the ground truth rather than the enhanced fragment. As a result, we can observe some color inconsistency between the cropped part and the recovered contents in the upper two examples. It further proves that CLR-Net focuses on fidelity rather than feasibility during image recovery. Table II also reports quantitative results on untrained attacks, where the performance gaps between trained attacks and untrained ones are acceptable.

Performance trade-off. If more information is embedded into the original image, we can expect more precise image recovery. However, too much information embedding will deteriorate the quality of the protected image, so there is a performance trade-off. In Fig. 9, we provide the PSNR curve which reports the average PSNR between the original and protected images versus the average PSNR between the original and recovered images. We report the experimental results on images sized 256×256 from MS-COCO dataset, and the other resolutions and datasets share similar trends. We see that the quality of the recovered image does not improve much if the PSNR of the protected image is less than 32.5dB, but it plummets if it is larger than 33dB. Therefore, when PSNR is close to 32.5dB, the trade-off can be well balanced. Otherwise, either the quality of the protected image or the recovered image will be not satisfactory.

Performance on different resolutions. Table III shows the average results for images with different resolution. We conduct experiments by using fixed survival rate $r_c = 0.7^2$. Note that although we train a unified model for different datasets and attacks, we train separate models for different

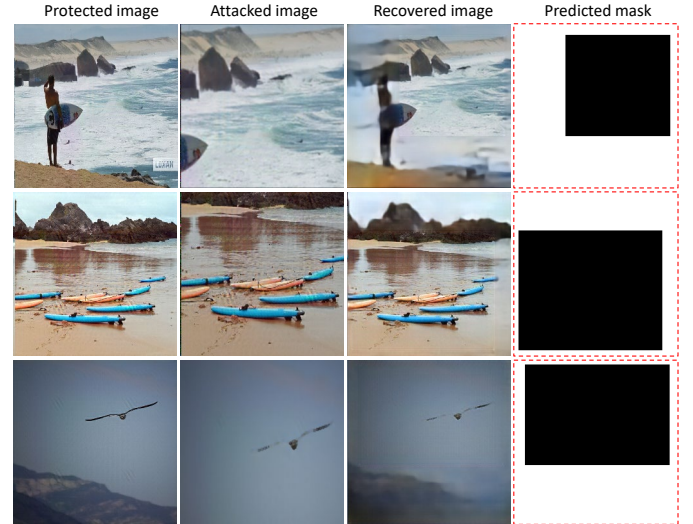


Fig. 10. Experimental results on extreme cases, where the volunteers deliberately remove some critical objects within the images. Attack type: JPEG (QF=80).

resolutions. Combined with Table. I, we find that CLR-Net comprehensively performs the best on 128×128 -sized images and performs the worst on 512×512 -sized images, which indicates a performance drop with the image size going up. The reason is two-folded. First, larger images contain more higher-frequent details to be protected. Though larger images allow more room for data embedding, PSNR is especially sensitive to the mean-squared error. Second, larger resolutions also require more accurate estimations on the cropping masks, which is also harder to be ensured.

Human visual system analysis. Besides the above objective quality analysis, we further conduct subjective quality analysis by inviting ten volunteers to do the human visual system analysis. The evaluation process is designed as distinguishing the original images from the generated recovered images. To be specific, for each volunteer, we provide them with 100 recovered images and 100 original images. The recovered images are not related to the original images. Given a doubted image, the volunteers tell whether it is crude or generated. The result is that 42, or near a half, of the generated recovered images are mistaken for being the original images. Also, six original images are mistaken for being the recovered images, mainly due to poor image quality. The result verifies the satisfying quality of the recovered images.

Extreme cases. Besides the above tests, we further show some extreme cases where we deliberately remove complete items from the protected images. Fig. 10 showcases three examples, where the person in the first example and the mountain in the second example are completely missing. By observing the cropped image, we can infer that the recovery of the removed items should only rely on the embedded watermark, and deep image prior can hardly retrieve these items since there is little clue within the remaining image. From the results, we see that the missing contents are largely recovered, though some details are lost. Such ability cannot be achieved by any state-of-the-art image-reconstruction-based schemes.

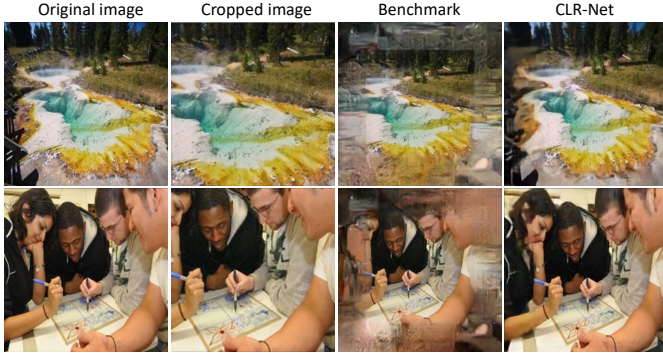


Fig. 11. **Comparison of CLR-Net with the benchmark on two JPEG images.** CLR-Net can preserve much better image fidelity where the recovered contents are not hallucinated.

TABLE IV

PERFORMANCE COMPARISON OF IMAGE CROPPING RECOVERY ON 200 DIFFERENT-RESOLUTIONED IMAGES FROM MS-COCO BETWEEN CLR-NET, BASELINE AND REGO [120]. SSIMS ARE IN THE BRACKETS.

Method	Resolution		
	512 ²	256 ²	128 ²
CLR-Net	28.11 (0.867)	29.57 (0.873)	31.30 (0.912)
Benchmark	17.02 (0.588)	19.42 (0.615)	21.67 (0.672)
ReGO [120]	19.24 (0.653)	18.75 (0.594)	27.17 (0.725)

C. Comparison

Image recovery from image cropping. The comparison result with the benchmark is shown in Fig. 11. Though we implement the benchmark using the state-of-the-art image recovery scheme, the results are both blurry and largely biased from the ground-truth image. Besides, we can clearly observe the border between the preserved contents and the recovered contents. In comparison, CLR-Net preserves better image fidelity and quality where the missing contents are truthfully recovered. We have implemented the benchmark using other state-of-the-art image outpainting networks and the results are close. It proves that we cannot apply the off-the-shelf image recovery schemes to replace CLR-Net, in that little intrinsic clue can be found in an image to recover the cropped-out areas. Therefore, it proves to be essential to reformulate Eq. (2) by introducing robust watermarking using $f_{prt}(\cdot)$.

For quantitative analysis, we arbitrarily select 200 images and freely crop them with $r_s \in [0.6, 1]$, and respectively use CLR-Net, the baseline and ReGO [120], another representative passive-based image outpainting and harmonization scheme, to recover the whole image. We conduct the experimental comparisons under three resolutions. According to the results reported in Table IV, the performance of CLR-Net leads by a large margin. While ReGo [120] can provide a much closer result when the input image is small-sized, the fidelity cannot be ensured for both the baseline and ReGO where the averaged PSNRs for these two schemes are all below 20dB when the resolution is larger.

Cropping identification and localization. Image cropping localization is historically less investigated because traces left by cropping is very subtle and fragile [66]. So far, the state

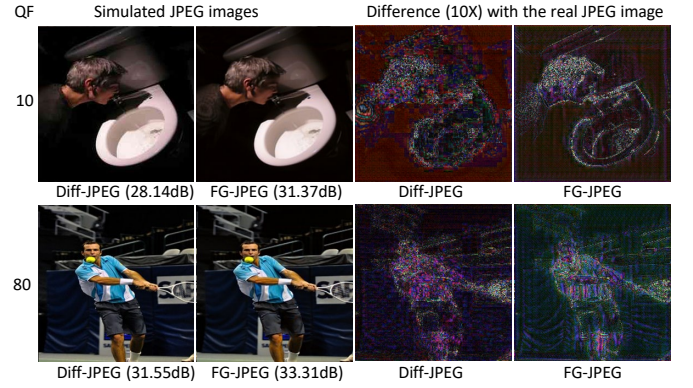


Fig. 12. **Comparison on the fidelity of the simulated JPEG images between FG-JPEG and Diff-JPEG [82].** The quality factor is respectively 10 in the first row and 80 in the second row. FG-JPEG contains less artifacts and compared with Diff-JPEG, and the outputs are more close to the ground truth compressed image.

TABLE V

COMPARISON OF DIFFERENT JPEG SIMULATORS BY MEASURING THE AVERAGE PSNR BETWEEN THE GROUND-TRUTH AND SIMULATED JPEG IMAGES (QF=70).

	FG-JPEG	Diff-JPEG	JPEG-Mask	JPEG-SS
PSNR	32.55	31.42	28.49	30.77
Accuracy	93.17%	72.48%	64.55%	73.42%

of the art in passive image cropping prediction accuracy is held by Van et al. [66], whose overall accuracy is reported to be 86% on uncompressed images. Whenever the input images are compressed or tainted by other digital attacks, the scheme can no longer predict the cropping mask. In our previous work [84], we are the first to use robust watermarking for image cropping localization, and the overall accuracy is 90.75% on natural images, regardless of whether the images are compressed or not. It is well notifying that both CLR-Net and [35] require proactively embedding information into the original images, which is different from Van et al. [66].

The cropping prediction accuracy of CLR-Net is 95.41% that further leads by a large margin. Note that in the result we include the false alarm rate where we should not predict *positive* on non-cropped images. For cropping localization, CLR-Net does not have restrictions on the quality or format of the targeted image, which is in line with [35]. For [66], since the statistical clue of lens artifacts are prone to image processing, the scheme is not applicable on the majority of natural images. According to Table II, the F1 scores of CLR-Net under JPEG (QF = 70) is within [0.94, 0.98], which is also higher than 0.74 reported in [84]. We owe the high accuracy of image cropping detection of CLR-Net to robust watermarking.

D. Ablation study

Fig. 12 and Table. V respectively provide qualitative and quantitative experiments where we compare FG-JPEG with Diff-JPEG [82], JPEG-Mask [13] and JPEG-SS [36]. Fig. 13 and Table VI respectively showcase and provide average results from several partial setups. In each ablation test, we

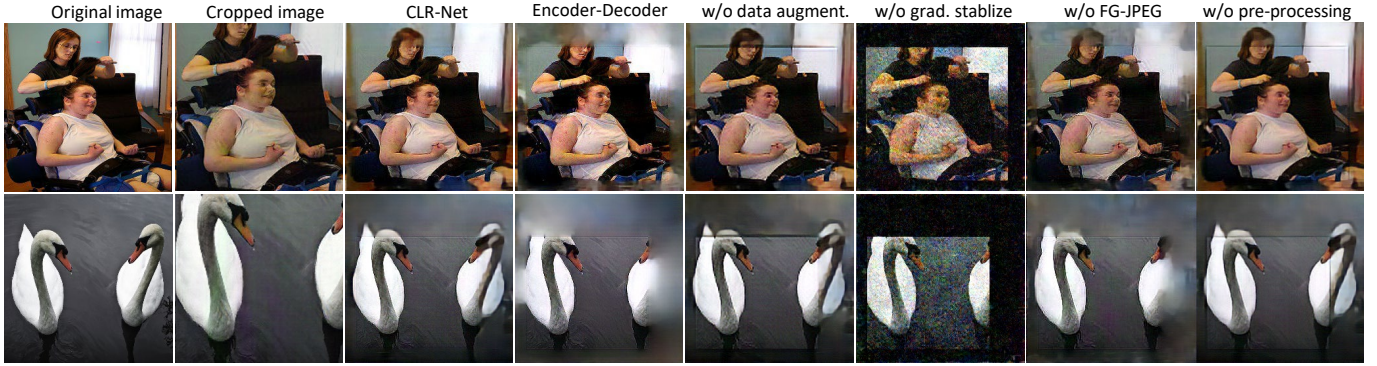


Fig. 13. **Ablation studies of CLR-Net from the view of image recovery.** The performances from the partial setups have noticeable gaps with the full implementation, which verifies the necessity of the network design and the training strategies. Especially, we cannot obtain a satisfactory result if we conduct image protection and recovery using separate encoder and decoder networks.

TABLE VI

AVERAGED RESULTS OF ABLATION STUDY ON MS-COCO AND FLICKER. THE TESTS ARE DONE UNDER JPEG ATTACK (QF=70) AND $r_c = 0.7^2$.

Setting	MS-COCO			Flicker		
	F1	PSNR	SSIM	F1	PSNR	SSIM
w/o anti-cropping protection ($\mathbf{I} = \mathbf{X}$)	0.435	18.13	0.585	0.393	15.46	0.374
w/o multi-staged training and synchronization	0.268	11.35	0.244	0.163	7.49	0.228
w/o gradient stabilization (do not prevent gradient explosion)	0.624	16.73	0.527	0.255	10.09	0.297
w/o image pre-processing ($\hat{\mathbf{X}}_{atk} = \mathbf{X}_{atk}$)	0.958	24.12	0.736	0.923	23.77	0.780
w/o tamper-based data augmentation	0.802	23.61	0.701	0.844	24.65	0.762
separate \mathbf{G} using two U-Net-based architecture	0.933	21.54	0.713	0.917	20.20	0.659
\mathbf{A} using JPEG-Mask [13]	0.917	22.47	0.678	0.923	23.07	0.699
\mathbf{A} using Diff-JPEG [82]	0.958	25.95	0.814	0.942	26.37	0.827
CLR-Net (Full implementation)	0.965	27.02	0.822	0.958	26.94	0.820

fine-tune CLR-Net till the accuracy of cropping localization is close to the baseline. We also use fixed attacks during testing. We discuss the influences of the network design and the training strategies.

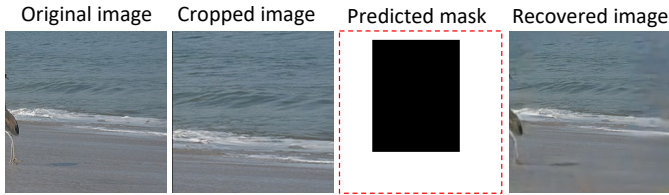
Influence of JPEG simulator. From Fig. 12, the PSNR results suggest that our generative method gives closer results to the real-world JPEG images. The averaged comparison results are shown in Table. V. We see that the averaged QF classification accuracy of Diff-JPEG is 72.48%, while that of FG-JPEG is 93.17%. It indicates that more knowledge about JPEG compression is learned by FG-JPEG with the joint guidance of the generative model and the QF predictor. Besides, the chess-board artifact of JPEG compression can also be found in the generated JPEG images, which owes to the strong capability of neural networks in learning representations. Fig. 13 shows that using Diff-JPEG in CLR-Net leads to blurry results. The reason is that CLR-Net is overfitted to the fixed compression mode provided by Diff-JPEG. In comparison, with a well-trained predictor, the network design enforces the FG-JPEG to generate more realistic JPEG images compared to Diff-JPEG. We further conduct ablation studies where we use the JPEG-Mask [13] and Mixup-JPEG [84] as the JPEG simulator to train our network. According to the results provided in Table VI, these settings also give inferior performances.

Influence of INN architecture. A typical alternative is to model image protection and image recovery independently

using the traditional *encoder-decoder* networks. Thus, we implement the image protection network and the image recovery network using two simple U-Nets [16]. For a fair comparison, we regulate that the two networks contain the same number of parameters in sum with CLR-Net. From Table VI, we observe that INN-based CLR-Net provides a better performance with a large margin. It owes to the fact that INNs learn stable invertible distribution mapping, where the forward and back propagation operations are in the same network.

Influence of tampering-based data augmentation. Our novel data augmentation based on tampering evenly and arbitrarily adds irrelevant information from different images to prevent the network from using spatial redundancy. This principle can not be borrowed from previous data augmentation methods such as Cut-Mix [76], Mix-up [32], etc. We find that without the proposed tamper-based data augmentation, CLR-Net tends to produce approximate and blurry recovery results, though the effect on cropping localization is trivial. It is especially the case on datasets like CelebA and ImageNet where the DIP is strong. The reason is that automatic cropping during training cannot always efficiently discard critical information, therefore offering a shortcut for the network to use DIP for recovery. We see a much lower quality and fidelity compared to CLR-Net.

Influence of multi-stage training and gradient stabilization. Fig. 13 shows that if we do not apply multi-staged training and



Application I: Reversible image cropping (the missing bird is recovered).



Application II: Image crop forgery detection (seeing where the boys are).

Fig. 14. **Application of CLR-Net.** The scheme can invert image crops without saving a copied version of the original image. Besides, CLR-Net is effective in image cropping forgery detection.

synchronization, CLR-Net has to adjust itself to an imperfect predicted mask. From the results, the network failed to come to any solution where the gradient exploded during training. A similar result happens when we do not apply the gradient stabilization. Therefore, it highlights the importance of necessary simplifications of the network flow and necessary task decomposition.

Influence of image pre-processor. We see a promising performance gain by the image pre-processing using the Siamese network. It proves that the network can help unifying \mathbf{I}_{atk} made by different benign attacks, which usually follows different distributions. For example, JPEG images have chessboard artifacts while brightness change mainly alters the mean value. Image pre-processing allows the generator to work on a more clustered transformed domain.

V. APPLICATIONS

Fig. 14 shows two examples of the real-world applications of CLR-Net. The first possible application of CLR-Net is reversible image editing. Traditionally, when we crop an image, the original version is either deleted for good or can be visited with the cost of additional memory cost. We propose to apply CLR-Net as an effective alternative, which can both do the opposite of the cropping and resist typical image processing attacks. Once we regret having cropped an image and wish to go back to the original version, we apply CLR-Net to recover the original image. For example, the cropped-out bird can be recovered by CLR-Net after its removal.

The second application is anti-cropping forgery detection, since CLR-Net can both identify image cropping and recover the original contents. In the lower example of Fig. 14, we suppose that a boy wants to deceive his mother by not telling her where today he has been. However, his cellphone has been equipped with CLR-Net by his mother, where every captured image will be first protected ahead of storage. So the mum localizes the cropped region and recovers the whole image. Though the recovered image is still an estimate of the original image, she can still generally know when and where

the boy was. The example shows the capability of exposing the cropped-out crucial information for image forgery detection.

VI. CONCLUSION

This paper proposes a novel robust watermarking scheme named CLR-NET for image crop localization and recovery. We formulate entire image recovery as the inverse of cropping and model the problem upon an INN-based anti-crop generator as well as a crop localizer. We propose two plug-in-and-play gadgets in our network to enhance real-world robustness. First, a novel Fine-Grained generative JPEG simulator (FG-JPEG) is used to flexibly mimic the characteristics of JPEG compression. Second, a Siamese network is proposed for image pre-processing on the attacked images where we minimize the performance gap against two different attacks in each iteration. Comprehensive experiments prove that the quality of the recovered image and the accuracy of crop localization are both satisfactory. Besides, CLR-NET can resist typical image attacks, where the novel FG-JPEG as well as the image pre-processor help promote real-world robustness. In future works, the performance of CLR-Net might be improved with the introduction of long-range attention-based mechanisms.

REFERENCES

- [1] J. Tao, S. Li, X. Zhang, and Z. Wang, "Towards robust image steganography," *IEEE Transactions on Circuits and Systems for Video Technology*, vol. 29, no. 2, pp. 594–600, 2018.
- [2] V. Sedighi, R. Cogranne, and J. Fridrich, "Content-adaptive steganography by minimizing statistical detectability," *IEEE Transactions on Information Forensics and Security*, vol. 11, no. 2, pp. 221–234, 2015.
- [3] K. Chen, H. Zhou, W. Zhou, W. Zhang, and N. Yu, "Defining cost functions for adaptive jpeg steganography at the microscale," *IEEE Transactions on Information Forensics and Security*, vol. 14, no. 4, pp. 1052–1066, 2018.
- [4] H. Fang, W. Zhang, H. Zhou, H. Cui, and N. Yu, "Screen-shooting resilient watermarking," *IEEE Transactions on Information Forensics and Security*, vol. 14, no. 6, pp. 1403–1418, 2018.
- [5] N. Agarwal, A. K. Singh, and P. K. Singh, "Survey of robust and imperceptible watermarking," *Multimedia Tools and Applications*, vol. 78, no. 7, pp. 8603–8633, 2019.
- [6] M. Asikuzzaman and M. R. Pickering, "An overview of digital video watermarking," *IEEE Transactions on Circuits and Systems for Video Technology*, vol. 28, no. 9, pp. 2131–2153, 2017.
- [7] Y.-Q. Shi, X. Li, X. Zhang, H.-T. Wu, and B. Ma, "Reversible data hiding: advances in the past two decades," *IEEE access*, vol. 4, pp. 3210–3237, 2016.
- [8] S. Baluja, "Hiding images in plain sight: Deep steganography," *Advances in Neural Information Processing Systems*, vol. 30, pp. 2069–2079, 2017.
- [9] —, "Hiding images within images," *IEEE Transactions on Pattern Analysis and Machine Intelligence*, 2019.
- [10] X. Duan, K. Jia, B. Li, D. Guo, E. Zhang, and C. Qin, "Reversible image steganography scheme based on a u-net structure," *IEEE Access*, vol. 7, pp. 9314–9323, 2019.
- [11] R. Rahim, S. Nadeem *et al.*, "End-to-end trained cnn encoder-decoder networks for image steganography," in *Proceedings of the European Conference on Computer Vision (ECCV)*, 2018, pp. 0–0.
- [12] H. Kandi, D. Mishra, and S. R. S. Gorthi, "Exploring the learning capabilities of convolutional neural networks for robust image watermarking," *Computers & Security*, vol. 65, pp. 247–268, 2017.
- [13] J. Zhu, R. Kaplan, J. Johnson, and L. Fei-Fei, "Hidden: Hiding data with deep networks," in *Proceedings of the European Conference on Computer Vision (ECCV)*, 2018, pp. 657–672.
- [14] X. Luo, R. Zhan, H. Chang, F. Yang, and P. Milanfar, "Distortion agnostic deep watermarking," in *Proceedings of the IEEE/CVF Conference on Computer Vision and Pattern Recognition*, 2020, pp. 13 548–13 557.

- [15] X. Bi, Y. Liu, B. Xiao, W. Li, C.-M. Pun, G. Wang, and X. Gao, "D-unet: A dual-encoder u-net for image splicing forgery detection and localization," *arXiv preprint arXiv:2012.01821*, 2020.
- [16] O. Ronneberger, P. Fischer, and T. Brox, "U-net: Convolutional networks for biomedical image segmentation," in *International Conference on Medical image computing and computer-assisted intervention*. Springer, 2015, pp. 234–241.
- [17] C. Szegedy, V. Vanhoucke, S. Ioffe, J. Shlens, and Z. Wojna, "Rethinking the inception architecture for computer vision," in *Proceedings of the IEEE conference on computer vision and pattern recognition*, 2016, pp. 2818–2826.
- [18] P. Isola, J.-Y. Zhu, T. Zhou, and A. A. Efros, "Image-to-image translation with conditional adversarial networks," in *Proceedings of the IEEE Conference on Computer Vision and Pattern Recognition*, 2017, pp. 1125–1134.
- [19] J. Johnson, A. Alahi, and L. Fei-Fei, "Perceptual losses for real-time style transfer and super-resolution," in *European Conference on Computer Vision*. Springer, 2016, pp. 694–711.
- [20] L. I. Rudin, S. Osher, and E. Fatemi, "Nonlinear total variation based noise removal algorithms," *Physica D: nonlinear phenomena*, vol. 60, no. 1–4, pp. 259–268, 1992.
- [21] T.-Y. Lin, M. Maire, S. Belongie, J. Hays, P. Perona, D. Ramanan, P. Dollár, and C. L. Zitnick, "Microsoft coco: Common objects in context," in *European Conference on Computer Vision*. Springer, 2014, pp. 740–755.
- [22] J. Deng, W. Dong, R. Socher, L.-J. Li, K. Li, and L. Fei-Fei, "Imagenet: A large-scale hierarchical image database," in *2009 IEEE conference on computer vision and pattern recognition*. Ieee, 2009, pp. 248–255.
- [23] P. Lu, H. Zhang, X. Peng, and X. Jin, "Learning the relation between interested objects and aesthetic region for image cropping," *IEEE Transactions on Multimedia*, vol. 23, pp. 3618–3630, 2020.
- [24] C. De Vleeschouwer, J.-F. Delaigle, and B. Macq, "Circular interpretation of bijective transformations in lossless watermarking for media asset management," *IEEE Transactions on Multimedia*, vol. 5, no. 1, pp. 97–105, 2003.
- [25] X. Zhang and S. Wang, "Fragile watermarking with error-free restoration capability," *IEEE Transactions on Multimedia*, vol. 10, no. 8, pp. 1490–1499, 2008.
- [26] R. Geirhos, J.-H. Jacobsen, C. Michaelis, R. Zemel, W. Brendel, M. Bethge, and F. A. Wichmann, "Shortcut learning in deep neural networks," *Nature Machine Intelligence*, vol. 2, no. 11, pp. 665–673, 2020.
- [27] Z. Wang, A. C. Bovik, H. R. Sheikh, and E. P. Simoncelli, "Image quality assessment: from error visibility to structural similarity," *IEEE Transactions on Image Processing*, vol. 13, no. 4, pp. 600–612, 2004.
- [28] C. Yu, "Attention based data hiding with generative adversarial networks," in *Proceedings of the AAAI Conference on Artificial Intelligence*, vol. 34, no. 01, 2020, pp. 1120–1128.
- [29] X. Mao, Q. Li, H. Xie, R. Y. Lau, Z. Wang, and S. Paul Smolley, "Least squares generative adversarial networks," in *Proceedings of the IEEE International Conference on Computer Vision*, 2017, pp. 2794–2802.
- [30] S. Ioffe and C. Szegedy, "Batch normalization: Accelerating deep network training by reducing internal covariate shift," in *International conference on machine learning*. PMLR, 2015, pp. 448–456.
- [31] N. Carlini and D. Wagner, "Towards evaluating the robustness of neural networks," in *2017 IEEE symposium on security and privacy (sp)*. IEEE, 2017, pp. 39–57.
- [32] H. Zhang, M. Cisse, Y. N. Dauphin, and D. Lopez-Paz, "mixup: Beyond empirical risk minimization," *arXiv preprint arXiv:1710.09412*, 2017.
- [33] D. Khachaturov, I. Shumailov, Y. Zhao, N. Papernot, and R. Anderson, "Markpainting: Adversarial machine learning meets inpainting," in *International Conference on Machine Learning*. PMLR, 2021, pp. 5409–5419.
- [34] M. Yin, Y. Zhang, X. Li, and S. Wang, "When deep fool meets deep prior: Adversarial attack on super-resolution network," in *Proceedings of the 26th ACM International Conference on Multimedia*, 2018, pp. 1930–1938.
- [35] Q. Ying, Z. Qian, H. Zhou, H. Xu, X. Zhang, and S. Li, "From image to image: Immunized image generation," in *Proceedings of the 29th ACM international conference on Multimedia*, 2021, pp. 1–9.
- [36] K. Liu, D. Chen, J. Liao, W. Zhang, H. Zhou, J. Zhang, W. Zhou, and N. Yu, "Jpeg robust invertible grayscale," *IEEE Transactions on Visualization and Computer Graphics*, 2021.
- [37] Z. Jia, H. Fang, and W. Zhang, "Mbrs: Enhancing robustness of dnn-based watermarking by mini-batch of real and simulated jpeg compression," *arXiv preprint arXiv:2108.08211*, 2021.
- [38] D.-A. Clevert, T. Unterthiner, and S. Hochreiter, "Fast and accurate deep network learning by exponential linear units (elus)," *arXiv preprint arXiv:1511.07289*, 2015.
- [39] F. Yu and V. Koltun, "Multi-scale context aggregation by dilated convolutions," *arXiv preprint arXiv:1511.07122*, 2015.
- [40] D. P. Kingma and J. Ba, "Adam: A method for stochastic optimization," *arXiv preprint arXiv:1412.6980*, 2014.
- [41] H. Cheng and X. Shi, "A simple and effective histogram equalization approach to image enhancement," *Digital signal processing*, vol. 14, no. 2, pp. 158–170, 2004.
- [42] A. Bruhn, J. Weickert, and C. Schnörr, "Lucas/kanade meets horn/schunck: Combining local and global optic flow methods," *IJCV*, vol. 61, no. 3, pp. 211–231, 2005.
- [43] H. Bay, T. Tuytelaars, and L. Van Gool, "Surf: Speeded up robust features," in *European Conference on Computer Vision*. Springer, 2006, pp. 404–417.
- [44] W. Li, Y. Yuan, and N. Yu, "Passive detection of doctored jpeg image via block artifact grid extraction," *Signal Processing*, vol. 89, no. 9, pp. 1821–1829, 2009.
- [45] D. G. Lowe, "Object recognition from local scale-invariant features," in *Proceedings of the seventh IEEE international conference on computer vision*, vol. 2. Ieee, 1999, pp. 1150–1157.
- [46] S.-Y. Wang, O. Wang, R. Zhang, A. Owens, and A. A. Efros, "Cnn-generated images are surprisingly easy to spot... for now," in *Proceedings of the IEEE/CVF Conference on Computer Vision and Pattern Recognition*, 2020, pp. 8695–8704.
- [47] H. Lu, R. Shen, and F.-L. Chung, "Fragile watermarking scheme for image authentication," *Electronics Letters*, vol. 39, no. 12, pp. 898–900, 2003.
- [48] H. He, J. Zhang, and H.-M. Tai, "A wavelet-based fragile watermarking scheme for secure image authentication," in *International Workshop on Digital Watermarking*. Springer, 2006, pp. 422–432.
- [49] X. Zhang, S. Wang, Z. Qian, and G. Feng, "Self-embedding watermark with flexible restoration quality," *Multimedia Tools and Applications*, vol. 54, no. 2, pp. 385–395, 2011.
- [50] X. Zhang and S. Wang, "Fragile watermarking scheme using a hierarchical mechanism," *Signal processing*, vol. 89, no. 4, pp. 675–679, 2009.
- [51] P. Korus and A. Dziech, "Efficient method for content reconstruction with self-embedding," *IEEE Transactions on Image Processing*, vol. 22, no. 3, pp. 1134–1147, 2012.
- [52] X. Zhang, Z. Qian, and G. Feng, "Reference sharing mechanism for watermark self-embedding," *IEEE Transactions on Image Processing*, vol. 20, no. 2, pp. 485–495, 2010.
- [53] X. Zhang, Z. Qian, Y. Ren, and G. Feng, "Watermarking with flexible self-recovery quality based on compressive sensing and compositive reconstruction," *IEEE Transactions on Information Forensics and Security*, vol. 6, no. 4, pp. 1223–1232, 2011.
- [54] L. Verdoliva, "Media forensics and deepfakes: an overview," *IEEE Journal of Selected Topics in Signal Processing*, vol. 14, no. 5, pp. 910–932, 2020.
- [55] X. Bi, Y. Wei, B. Xiao, and W. Li, "Rru-net: The ringed residual u-net for image splicing forgery detection," in *Proceedings of the IEEE/CVF Conference on Computer Vision and Pattern Recognition Workshops*, 2019, pp. 0–0.
- [56] Y. Wu, W. AbdAlmageed, and P. Natarajan, "Mantra-net: Manipulation tracing network for detection and localization of image forgeries with anomalous features," in *Proceedings of the IEEE/CVF Conference on Computer Vision and Pattern Recognition*, 2019, pp. 9543–9552.
- [57] F. Chen, H. He, and Y. Huo, "Self-embedding watermarking scheme against jpeg compression with superior imperceptibility," *Multimedia Tools and Applications*, vol. 76, no. 7, pp. 9681–9712, 2017.
- [58] R. Preda and D. Vizireanu, "Watermarking-based image authentication robust to jpeg compression," *Electronics Letters*, vol. 51, no. 23, pp. 1873–1875, 2015.
- [59] M.-J. Tsai and C.-C. Chien, "Authentication and recovery for wavelet-based semifragile watermarking," *Optical Engineering*, vol. 47, no. 6, p. 067005, 2008.
- [60] L. Li, J. Bao, T. Zhang, H. Yang, D. Chen, F. Wen, and B. Guo, "Face x-ray for more general face forgery detection," in *Proceedings of the IEEE/CVF Conference on Computer Vision and Pattern Recognition*, 2020, pp. 5001–5010.
- [61] I. Yerushalmy and H. Hel-Or, "Digital image forgery detection based on lens and sensor aberration," *International Journal of Computer Vision*, vol. 92, no. 1, pp. 71–91, 2011.

- [62] A. R. Bruna, G. Messina, and S. Battiato, "Crop detection through blocking artefacts analysis," in *International Conference on Image Analysis and Processing*. Springer, 2011, pp. 650–659.
- [63] Y. Huang, B. Niu, H. Guan, and S. Zhang, "Enhancing image watermarking with adaptive embedding parameter and psnr guarantee," *IEEE Transactions on Multimedia*, vol. 21, no. 10, pp. 2447–2460, 2019.
- [64] R. Liu and T. Tan, "An svd-based watermarking scheme for protecting rightful ownership," *IEEE Transactions on Multimedia*, vol. 4, no. 1, pp. 121–128, 2002.
- [65] M. Fanfani, M. Iuliani, F. Bellavia, C. Colombo, and A. Piva, "A vision-based fully automated approach to robust image cropping detection," *Signal Processing: Image Communication*, vol. 80, p. 115629, 2020.
- [66] B. Van Hoorick and C. Vondrick, "Dissecting image crops," in *Proceedings of the IEEE/CVF International Conference on Computer Vision*, 2021, pp. 9741–9750.
- [67] B. Van Hoorick, "Image outpainting and harmonization using generative adversarial networks," *arXiv preprint arXiv:1912.10960*, 2019.
- [68] I. J. Goodfellow, J. Pouget-Abadie, M. Mirza, B. Xu, D. Warde-Farley, S. Ozair, A. Courville, and Y. Bengio, "Generative adversarial networks," *arXiv preprint arXiv:1406.2661*, 2014.
- [69] S.-M. Mun, S.-H. Nam, H. Jang, D. Kim, and H.-K. Lee, "Finding robust domain from attacks: A learning framework for blind watermarking," *Neurocomputing*, vol. 337, pp. 191–202, 2019.
- [70] L. Dinh, D. Krueger, and Y. Bengio, "Nice: Non-linear independent components estimation," *arXiv preprint arXiv:1410.8516*, 2014.
- [71] L. Dinh, J. Sohl-Dickstein, and S. Bengio, "Density estimation using real nvp," *arXiv preprint arXiv:1605.08803*, 2016.
- [72] D. P. Kingma and P. Dhariwal, "Glow: Generative flow with invertible 1x1 convolutions," *Advances in Neural Information Processing Systems*, vol. 31, 2018.
- [73] R. Zhao, T. Liu, J. Xiao, D. P. Lun, and K.-M. Lam, "Invertible image decolorization," *IEEE Transactions on Image Processing*, vol. 30, pp. 6081–6095, 2021.
- [74] M. Xiao, S. Zheng, C. Liu, Y. Wang, D. He, G. Ke, J. Bian, Z. Lin, and T.-Y. Liu, "Invertible image rescaling," in *European Conference on Computer Vision*. Springer, 2020, pp. 126–144.
- [75] Y. Xing, Z. Qian, and Q. Chen, "Invertible image signal processing," in *Proceedings of the IEEE/CVF Conference on Computer Vision and Pattern Recognition*, 2021, pp. 6287–6296.
- [76] S. Yun, D. Han, S. J. Oh, S. Chun, J. Choe, and Y. Yoo, "Cutmix: Regularization strategy to train strong classifiers with localizable features," in *Proceedings of the IEEE/CVF international conference on computer vision*, 2019, pp. 6023–6032.
- [77] S.-P. Lu, R. Wang, T. Zhong, and P. L. Rosin, "Large-capacity image steganography based on invertible neural networks," in *Proceedings of the IEEE/CVF Conference on Computer Vision and Pattern Recognition*, 2021, pp. 10816–10825.
- [78] R. O. Park E, Liu W, "Ilsrvc-2017," 2017. [Online]. Available: <http://www.image-net.org/challenges/LSVRC/2017>
- [79] T. Karras, T. Aila, S. Laine, and J. Lehtinen, "Progressive growing of gans for improved quality, stability, and variation," *arXiv preprint arXiv:1710.10196*, 2017.
- [80] N. Liu, P. Amin, and K. Subbalakshmi, "Security and robustness enhancement for image data hiding," *IEEE Transactions on Multimedia*, vol. 9, no. 3, pp. 466–474, 2007.
- [81] Q. Ying, J. Lin, Z. Qian, H. Xu, and X. Zhang, "Robust digital watermarking for color images in combined dft and dt-cwt domains," *Mathematical Biosciences and Engineering*, vol. 16, no. 5, pp. 4788–4801, 2019.
- [82] R. Shin and D. Song, "Jpeg-resistant adversarial images," in *NIPS 2017 Workshop on Machine Learning and Computer Security*, vol. 1, 2017.
- [83] T. Miyato, T. Kataoka, M. Koyama, and Y. Yoshida, "Spectral normalization for generative adversarial networks," *arXiv preprint arXiv:1802.05957*, 2018.
- [84] Q. Ying, X. Hu, H. Zhou, X. Zhang, Z. You, and Z. Qian, "No way to crop: On robust image crop localization," *arXiv preprint arXiv:2110.05687*, 2021.
- [85] J. Yu, Z. Lin, J. Yang, X. Shen, X. Lu, and T. S. Huang, "Generative image inpainting with contextual attention," in *Proceedings of the IEEE conference on computer vision and pattern recognition*, 2018, pp. 5505–5514.
- [86] N. Wang, J. Li, L. Zhang, and B. Du, "Musical: Multi-scale image contextual attention learning for inpainting," in *IJCAI*, 2019, pp. 3748–3754.
- [87] D. Ulyanov, A. Vedaldi, and V. Lempitsky, "Deep image prior," in *Proceedings of the IEEE Conference on Computer Vision and Pattern Recognition*, 2018, pp. 9446–9454.
- [88] A. Islam, C. Long, A. Basharat, and A. Hoogs, "Doa-gan: Dual-order attentive generative adversarial network for image copy-move forgery detection and localization," in *Proceedings of the IEEE/CVF Conference on Computer Vision and Pattern Recognition*, 2020, pp. 4676–4685.
- [89] G. Schaefer and M. Stich, "Ucid: An uncompressed color image database," in *Storage and Retrieval Methods and Applications for Multimedia 2004*, vol. 5307. International Society for Optics and Photonics, 2003, pp. 472–480.
- [90] E. Agustsson and R. Timofte, "Ntire 2017 challenge on single image super-resolution: Dataset and study," in *Proceedings of the IEEE conference on computer vision and pattern recognition workshops*, 2017, pp. 126–135.
- [91] K. He, G. Gkioxari, P. Dollár, and R. Girshick, "Mask r-cnn," in *Proceedings of the IEEE International Conference on Computer Vision*, 2017, pp. 2961–2969.
- [92] S. Ren, K. He, R. Girshick, and J. Sun, "Faster r-cnn: Towards real-time object detection with region proposal networks," *Advances in neural information processing systems*, vol. 28, pp. 91–99, 2015.
- [93] Z. Liu, P. Luo, X. Wang, and X. Tang, "Large-scale celebfaces attributes (celeba) dataset," *Retrieved August*, vol. 15, no. 2018, p. 11, 2018.
- [94] B. Zhou, A. Lapedriza, A. Khosla, A. Oliva, and A. Torralba, "Places: A 10 million image database for scene recognition," *IEEE transactions on pattern analysis and machine intelligence*, vol. 40, no. 6, pp. 1452–1464, 2017.
- [95] J. Behrmann, W. Grathwohl, R. T. Chen, D. Duvenaud, and J.-H. Jacobsen, "Invertible residual networks," in *International Conference on Machine Learning*. PMLR, 2019, pp. 573–582.
- [96] P. Zhou, X. Han, V. I. Morariu, and L. S. Davis, "Learning rich features for image manipulation detection," in *Proceedings of the IEEE Conference on Computer Vision and Pattern Recognition*, 2018, pp. 1053–1061.
- [97] B. Bayar and M. C. Stamm, "Constrained convolutional neural networks: A new approach towards general purpose image manipulation detection," *IEEE Transactions on Information Forensics and Security*, vol. 13, no. 11, pp. 2691–2706, 2018.
- [98] W. Grathwohl, R. T. Chen, J. Bettencourt, I. Sutskever, and D. Duvenaud, "Ffjord: Free-form continuous dynamics for scalable reversible generative models," *arXiv preprint arXiv:1810.01367*, 2018.
- [99] X. Chen, C. Dong, J. Ji, J. Cao, and X. Li, "Image manipulation detection by multi-view multi-scale supervision," *arXiv preprint arXiv:2104.06832*, 2021.
- [100] K. He, X. Zhang, S. Ren, and J. Sun, "Deep residual learning for image recognition," in *Proceedings of the IEEE conference on computer vision and pattern recognition*, 2016, pp. 770–778.
- [101] Y. Bengio, N. Léonard, and A. Courville, "Estimating or propagating gradients through stochastic neurons for conditional computation," *arXiv preprint arXiv:1308.3432*, 2013.
- [102] X. Wang, K. Yu, S. Wu, J. Gu, Y. Liu, C. Dong, Y. Qiao, and C. Change Loy, "Esrgan: Enhanced super-resolution generative adversarial networks," in *Proceedings of the European Conference on Computer Vision (ECCV) workshops*, 2018, pp. 0–0.
- [103] J. Jing, X. Deng, M. Xu, J. Wang, and Z. Guan, "Hinet: Deep image hiding by invertible network," in *Proceedings of the IEEE/CVF International Conference on Computer Vision*, 2021, pp. 4733–4742.
- [104] Y. Wang, L. Wang, J. Yang, W. An, and Y. Guo, "Flickr1024: A large-scale dataset for stereo image super-resolution," in *The IEEE International Conference on Computer Vision (ICCV) Workshops*, Oct 2019, pp. 3852–3857.
- [105] S. Pfennig and M. Kirchner, "Spectral methods to determine the exact scaling factor of resampled digital images," in *2012 5th International Symposium on Communications, Control and Signal Processing*. IEEE, 2012, pp. 1–6.
- [106] X. Chen and K. He, "Exploring simple siamese representation learning," in *Proceedings of the IEEE/CVF Conference on Computer Vision and Pattern Recognition*, 2021, pp. 15750–15758.
- [107] L. Wang, Y. Wang, Z. Liang, Z. Lin, J. Yang, W. An, and Y. Guo, "Learning parallax attention for stereo image super-resolution," in *Proceedings of the IEEE Conference on Computer Vision and Pattern Recognition*, 2019, p. 12250–12259.
- [108] L. Ardizzone, J. Kruse, S. Winkert, D. Rahner, E. W. Pellegrini, R. S. Klessen, L. Maier-Hein, C. Rother, and U. Köthe, "Analyzing inverse problems with invertible neural networks," *arXiv preprint arXiv:1808.04730*, 2018.
- [109] C. Zhang, A. Karjauv, P. Benz, and I. S. Kweon, "Towards robust deep hiding under non-differentiable distortions for practical blind wa-

- termarking," in *Proceedings of the 29th ACM International Conference on Multimedia*, 2021, pp. 5158–5166.
- [110] Q. Cheng and T. S. Huang, "Robust optimum detection of transform domain multiplicative watermarks," *IEEE Transactions on Signal Processing*, vol. 51, no. 4, pp. 906–924, 2003.
- [111] Y. Wang and A. Pearmain, "Blind mpeg-2 video watermarking robust against geometric attacks: a set of approaches in dct domain," *IEEE transactions on image processing*, vol. 15, no. 6, pp. 1536–1543, 2006.
- [112] Q. Ying, H. Zhou, X. Zeng, H. Xu, Z. Qian, and X. Zhang, "Hiding images into images with real-world robustness," *arXiv preprint arXiv:2110.05689*, 2021.
- [113] Y. Wang, Q. Ying, Z. Qian, S. Li, and X. Zhang, "A dtcwt-svd based video watermarking resistant to frame rate conversion," *arXiv preprint arXiv:2206.01094*, 2022.
- [114] Q. Liu, S. Yang, J. Liu, P. Xiong, and M. Zhou, "A discrete wavelet transform and singular value decomposition-based digital video watermark method," *Applied Mathematical Modelling*, vol. 85, pp. 273–293, 2020.
- [115] C.-C. Lai and C.-C. Tsai, "Digital image watermarking using discrete wavelet transform and singular value decomposition," *IEEE Transactions on instrumentation and measurement*, vol. 59, no. 11, pp. 3060–3063, 2010.
- [116] H. Mareen, J. De Praeter, G. Van Wallendael, and P. Lambert, "A scalable architecture for uncompressed-domain watermarked videos," *IEEE Transactions on Information Forensics and Security*, vol. 14, no. 6, pp. 1432–1444, 2018.
- [117] S. M. Pizer, E. P. Amburn, J. D. Austin, R. Cromartie, A. Geselowitz, T. Greer, B. ter Haar Romeny, J. B. Zimmerman, and K. Zuiderveld, "Adaptive histogram equalization and its variations," *Computer vision, graphics, and image processing*, vol. 39, no. 3, pp. 355–368, 1987.
- [118] J.-Y. Zhu, T. Park, P. Isola, and A. A. Efros, "Unpaired image-to-image translation using cycle-consistent adversarial networks," in *Proceedings of the IEEE International Conference on Computer Vision*, 2017, pp. 2223–2232.
- [119] Y. Xu, C. Mou, Y. Hu, J. Xie, and J. Zhang, "Robust invertible image steganography," in *Proceedings of the IEEE/CVF Conference on Computer Vision and Pattern Recognition*, 2022, pp. 7875–7884.
- [120] Y. Wang, Y. Wei, X. Qian, L. Zhu, and Y. Yang, "Rego: Reference-guided outpainting for scenery image," *arXiv preprint arXiv:2106.10601*, 2021.
- [121] Y.-C. Cheng, C. H. Lin, H.-Y. Lee, J. Ren, S. Tulyakov, and M.-H. Yang, "In&out: Diverse image outpainting via gan inversion," *arXiv preprint arXiv:2104.00675*, 2021.
- [122] Y. Wang, Y. Wei, X. Qian, L. Zhu, and Y. Yang, "Sketch-guided scenery image outpainting," *IEEE Transactions on Image Processing*, vol. 30, pp. 2643–2655, 2021.
- [123] K. Nazari, E. Ng, T. Joseph, F. Qureshi, and M. Ebrahimi, "Edge-connect: Structure guided image inpainting using edge prediction," in *Proceedings of the IEEE/CVF International Conference on Computer Vision Workshops*, 2019, pp. 0–0.
- [124] S. Iizuka, E. Simo-Serra, and H. Ishikawa, "Globally and locally consistent image completion," *ACM Transactions on Graphics (ToG)*, vol. 36, no. 4, pp. 1–14, 2017.
- [125] N. Otsu, "A threshold selection method from gray-level histograms," *IEEE transactions on systems, man, and cybernetics*, vol. 9, no. 1, pp. 62–66, 1979.
- [126] J. Fridrich, T. Pevný, and J. Kodovský, "Statistically undetectable jpeg steganography: dead ends challenges, and opportunities," in *Proceedings of the 9th workshop on Multimedia & security*, 2007, pp. 3–14.
- [127] T. Pevný, T. Filler, and P. Bas, "Using high-dimensional image models to perform highly undetectable steganography," in *International Workshop on Information Hiding*. Springer, 2010, pp. 161–177.
- [128] A. Cheddad, J. Condell, K. Curran, and P. Mc Kevitt, "Digital image steganography: Survey and analysis of current methods," *Signal processing*, vol. 90, no. 3, pp. 727–752, 2010.
- [129] I. Cox, M. Miller, J. Bloom, J. Fridrich, and T. Kalker, *Digital watermarking and steganography*. Morgan kaufmann, 2007.
- [130] J. Hayes and G. Danezis, "Generating steganographic images via adversarial training," *arXiv preprint arXiv:1703.00371*, 2017.
- [131] W. Tang, S. Tan, B. Li, and J. Huang, "Automatic steganographic distortion learning using a generative adversarial network," *IEEE Signal Processing Letters*, vol. 24, no. 10, pp. 1547–1551, 2017.
- [132] P. Wu, Y. Yang, and X. Li, "Stegnet: Mega image steganography capacity with deep convolutional network," *Future Internet*, vol. 10, no. 6, p. 54, Jun 2018. [Online]. Available: <http://dx.doi.org/10.3390/fi10060054>
- [133] K. A. Zhang, A. Cuesta-Infante, and K. Veeramachaneni, "Steganogan: Pushing the limits of image steganography," 2019.
- [134] E. Wengrowski and K. Dana, "Light field messaging with deep photographic steganography," in *Proceedings of the IEEE/CVF Conference on Computer Vision and Pattern Recognition*, 2019, pp. 1515–1524.
- [135] C. W. Park, Y. H. Moon, and I. K. Eom, "Image tampering localization using demosaicing patterns and singular value based prediction residue," *IEEE Access*, vol. 9, pp. 91 921–91 933, 2021.
- [136] N. Le and F. Retraint, "An improved algorithm for digital image authentication and forgery localization using demosaicing artifacts," *IEEE Access*, vol. 7, pp. 125 038–125 053, 2019.
- [137] J.-H. Choi, H. Zhang, J.-H. Kim, C.-J. Hsieh, and J.-S. Lee, "Evaluating robustness of deep image super-resolution against adversarial attacks," in *Proceedings of the IEEE/CVF International Conference on Computer Vision*, 2019, pp. 303–311.
- [138] R. Takahashi, T. Matsubara, and K. Uehara, "Data augmentation using random image cropping and patching for deep cnns," *IEEE Transactions on Circuits and Systems for Video Technology*, vol. 30, no. 9, pp. 2917–2931, 2019.
- [139] H. Wu, G. Liu, Y. Yao, and X. Zhang, "Watermarking neural networks with watermarked images," *IEEE Transactions on Circuits and Systems for Video Technology*, vol. 31, no. 7, pp. 2591–2601, 2020.
- [140] G. Feng, X. Zhang, Y. Ren, Z. Qian, and S. Li, "Diversity-based cascade filters for jpeg steganalysis," *IEEE transactions on circuits and systems for video technology*, vol. 30, no. 2, pp. 376–386, 2019.
- [141] Z. Qian, H. Xu, X. Luo, and X. Zhang, "New framework of reversible data hiding in encrypted jpeg bitstreams," *IEEE Transactions on Circuits and Systems for Video Technology*, vol. 29, no. 2, pp. 351–362, 2018.
- [142] N. Zhong, Z. Qian, Z. Wang, X. Zhang, and X. Li, "Batch steganography via generative network," *IEEE Transactions on Circuits and Systems for Video Technology*, vol. 31, no. 1, pp. 88–97, 2020.
- [143] P. Neekhar, B. Dolhansky, J. Bitton, and C. C. Ferrer, "Adversarial threats to deepfake detection: A practical perspective," in *Proceedings of the IEEE/CVF Conference on Computer Vision and Pattern Recognition*, 2021, pp. 923–932.
- [144] W. Huan, S. Li, Z. Qian, and X. Zhang, "Exploring stable coefficients on joint sub-bands for robust video watermarking in dt cwt domain," *IEEE Transactions on Circuits and Systems for Video Technology*, 2021.
- [145] T. Karras, S. Laine, and T. Aila, "A style-based generator architecture for generative adversarial networks," in *Proceedings of the IEEE/CVF Conference on Computer Vision and Pattern Recognition*, 2019, pp. 4401–4410.



Qichao Ying received the B.S. and M.S. degree from the School of Communication and Information Engineering, Shanghai University, China, respectively in 2017 and 2020. He is currently a doctoral candidate in the School of Computer Science, Fudan University, China. His research interests include forensics, steganography and watermarking for multimedia.



Hang Zhou received his B.S. degree in 2015 from Shanghai University and a Ph.D. degree in 2020 from the University of Science and Technology of China. Currently, he is a postdoctoral researcher at Simon Fraser University. His research interests include computer graphics, multimedia security and deep learning.



Zhenxing Qian graduated from University of Science and Technology of China (USTC), where he received the B.S. and Ph.D. degrees in 2003 and 2008, respectively. He is a Professor in the School of Computer Science, Fudan University, where he serves as the Vice Dean of the Key Lab of the China Culture & Tourism Ministry. His research interests include information hiding, multimedia security, and neural network security. Until now, he has published more than 160 peer-reviewed papers. Many of them are published IEEE TIFS, TMM, TDSC, TIP, TCSVT, TCYB, TCC, AAAI, IJCAI, ACM MM, etc. Besides, he is also an associate editor of “Signal Processing” & “Journal of Visual Communication and Image Representation”.



Sheng Li received the Ph.D. degree at the School of Electrical and Electronic Engineering, Nanyang Technological University, Singapore, in 2013. From 2013 to 2016, he was a research fellow in Rapid Rich Object Search (ROSE) Lab, Nanyang Technological University. He is currently an Associate Professor with the School of Computer Science, Fudan University, China. His research interests include biometric template protection, pattern recognition, multimedia forensics and security. He is the recipient of the IEEE WIFS Best Student Paper Silver Award.



Xinpeng Zhang received the B.S. degree in computational mathematics from Jilin University, China, in 1995, and the M.E. and Ph.D. degrees in communication and information system from Shanghai University, China, in 2001 and 2004, respectively, where he has been with the faculty of the School of Communication and Information Engineering, since 2004, and is currently a Professor. His research interests include information hiding, image processing, and digital forensics. He has published over 200 papers in these areas.